The effects of end wall profiling on secondary loss is a turbine nozzle row

Adamntois Gkiouvetsis

The Effects of End Wall Profiling on Secondary Loss is a Turbine Nozzle Row

By

Adamantios Gkiouvetsis

A thesis submitted in partial fulfillment of the requirements for the degree of Master of Science

School of Engineering
University of Durham
2000

Declaration

The work contained in this thesis has not been submitted elsewhere for any other degree or qualification, and unless otherwise referred it is the author's own work

Dedicated to my family and friends

Acknowledgements

I am most grateful to my supervisor Dr. David Gregory-Smith for his guidance and great help throughout this project.

I would also like to thank Mr. Jin Yan and Jonathan Hartland for their help as well as the technical staff in the school of engineering for their help in the Thermodynamics laboratory.

A warm thank also goes to my friend and colleague Miss Punithevaty Jayaraman for her help and support throughout my studies.

Finally I would like to thank Dr. Peter Walker and ALSTOM for their involvement in this project, which is greatly acknowledged.

The Effects of End Wall Profiling on Secondary Loss in a turbine Nozzle Row

Adamantios Gkiouvetsis

Abstract

This thesis presents detailed investigations of the effect of end wall profiling on the secondary loss in a turbine nozzle row. The purpose of this project was to obtain a detailed view of the flow structure downstream of the blade passage, especially of the area adjacent to the end wall, and the influence of the shaped end wall on both flow and loss.

The cascade was designed and manufactured by Yan [1999] based on nozzle blades by ALSTOM Energy Ltd. The low speed wind tunnel used by Yan was also used for the experimental work of this thesis, which were carried out in Durham thermodynamic laboratories. Two finer probes were used for the experiments allowing closer to the end wall measurements.

The flow field was investigated at exit from the blade row through two traverse slots. The secondary flow structure was understood and the effect of the profiled end wall was demonstrated by a reduction in the secondary loss and boundary layer thickness.

The data collected along with the previous work by Yan could be regarded as an indication of the possible advantages of end wall profiling in a real turbine. The next step would be to carry out similar work on real turbomachinery.

Contents

List of Figures

List of tables

Nomenclature

at	Half of the maximum change of shaped end wall
st	Distance between the peak of axial direction curvature and trailing edge
c	Chord
A	Area
C_L	Lift coefficient
h	Blade span
P	Static pressure
P_o	Total pressure
Y_S	Total pressure loss coefficient / Secondary loss coefficient
C_{po}	Total pressure loss coefficient[1]
C_p	Static pressure loss coefficient
Q	Dynamic pressure
s	blade pitch
V	Velocity
Vm	Mean velocity
X	Axial direction
$\dot{m}$	Mass flow rate
n	power low index
α	Flow angle (yaw angle)
β	Stagger angle
δ	Boundary layer thickness

[1] All coefficients are defined in the appendix

δ_1 Boundary layer displacement thickness

ρ Fluid density

Subscripts

1 Inlet

2 Outlet

ax Axial

Fs Free stream

s Streamwise direction

x Axial direction

l Local

u Upstream

Chapter 1:

Introduction

Advances in turbomachinery blade design have already achieved minimum profile losses, which make any efficiency improvement in two-dimensional cascades scarcely feasible. On the other hand secondary flows introduced by the three dimensional flow, which occur when the non-uniform flow is turned within a blade row, can be a great source of efficiency loss. Secondary flows can change the work output by a variation imposed on the exit angle. The increased losses and disturbance in the flow apart from the effect on the particular blade row can also increase losses downstream.

The damaging effect of secondary flow is more severe in low aspect ratio highly loaded turbine blade cascades where secondary flows account for up to half of the total loss. The importance of reducing secondary flows is evident and a lot of work has been carried out toward the reduction of such flows. Various methods have been

developed over the years amongst which end wall profiling is promising a decrease in loss, especially for nozzle blade rows, and an improvement in overall performance. Research by Deich [1960], Morris et.al. [1975] reported an increase in efficiency after testing various end wall configurations. Atkins [1987] stressed the need for a more systematic approach to end wall profiling design, and aided by CFD designed various end wall profiles which he tested

Yan et. al. [1999a] working on the same principles as Atkins on a project sponsored by ALSTOM investigated the effect of various end wall profiles on secondary flows using CFD. Experimental work by Yan et. al [1999b] was carried out after the profile, which produced the most desirable CFD results, was selected and manufactured. A linear cascade was designed and manufactured based on the ALSTOM nozzle guide vanes where both planar and profiled wall were tested and the effect of the profiled wall was investigated. Although a clear view of the flow field was achieved some distance from the end wall which showed reduction in secondary loss and secondary kinetic energy, there were no measurements in the area immediately adjacent to the end wall where it was believed that profiling should have a significant effect.

The aim of this project is to investigate the effect of the non-axisymmetric end wall profile produced by Yan et. al.[1999a] on the flow field close to the end wall so that the improvement reported by Yan et. al.[1999b] can be better quantified. The flow field downstream of the blade passage was investigated, both close to the end wall, using a small flattened pitot probe, and up to half the span, for planar and profiled end walls.

The work presented in this thesis covers the progress made over this research period and is divided in to six chapters, of which the first is this introductory chapter. The second chapter is a literature review of the main secondary flow mechanisms and control methods, including a discussion of end wall profiling. In the third chapter the instrumentation used is described along with the analysis procedures for the results which are presented in the fourth chapter. Chapter four includes the results for both profiled and planar end wall in comparison to results obtained by Yan et. al. [1999b, 1999c]. The fifth chapter provides an overview and discussion of this project. In the final chapter some conclusions are drawn and possible future work is discussed.

Chapter 2:

Review of Secondary Flow, Losses and Control Methods

The physical properties of secondary flows are described along with the methods of predicting the loss related to such flows. The main control techniques of secondary flows are reviewed and discussed. End wall profiling is also investigated and the current design of the end wall profile is described.

2.1 Secondary flows

Flow in axial turbomachinery is modelled simply as being two-dimensional. Development and research has shown that flow in axial turbomachinery differs from

the simple model of quasi two-dimensional flow that assumes a minor three-dimensional disturbance. In fact three-dimensional flow is very much in existence throughout the flow field. In highly loaded turbines where the turning of the flow is large, this effect can be a dominating feature within the blade passage. The two-dimensional mainstream flow is termed primary. The difference between the ideally two-dimensional primary flow and the actual flow is termed secondary flow. These secondary motions transverse to the main flow are responsible for the spiraling of the flow also observed around pipe bends. (Hawthorn [1955]).

Arising on annulus walls, or the end walls of a cascade, secondary flows are formed by the turning of the upstream boundary layer. The magnitude of loss associated with secondary flow, often termed as "end wall loss", and the strength of such flow depend mainly on two factors. According to Denton [1993] the factors effecting the strength and loss magnitude of secondary flows are the amount of turning the mainstream flow undergoes within blade row and the inlet boundary layer thickness. Although viscous forces are the reason for the formation of the boundary layer, their effect on secondary flow is of minor importance. The formation of secondary flow is attributed to pressure forces, so secondary flow is an invicid effect. Secondary flows can greatly reduce the efficiency of a turbomachine. In high pressure turbines, (low aspect ratio), where the turning of the flow is high, end wall losses are a major source of efficiency loss, contributing up to one third of the total loss (Denton [1993]). Furthermore the work output can be reduced as the exit angles are altered. The flow at exit from the blade row is highly turbulent and non-uniform. The non-uniformity of the flow causes unsteadiness and additional loss to the blade row downstream. In this manner loss is

accumulated from one blade row to an other and the overall effect of the secondary flow can be severe. Additionally secondary flow, apart from the aerodynamic effects can also have some effect the mechanical integrity of the blades as they are forced to work in off design conditions with increased vibration thus reducing their life expectancy.

2.2 Generation of secondary flows

In this section the secondary flow is discussed in terms of the main factors contributing to its generation and strength, within turbomachinery blade rows.

2.2.1 The pressure gradient

The boundary layer just upstream of the leading edge of the blade row is subjected to the pressure gradient existing between suction surface and pressure surface within a blade passage, set up by the mainstream flow. This can be described by the following equation:

$$\frac{\partial p}{\partial R} = \frac{\rho V^2}{R} \qquad \textbf{eq. 2.1}$$

Where **R** and **V** are the radius of curvature and velocity for the mainstream flow .On turning the slower moving fluid of the boundary layer is subjected to the same

pressure gradient as the faster moving mainstream flow. Applying the same equation for the slower moving fluid as well the following is derived

$$\frac{\partial p}{\partial R} = \frac{\rho V^2}{R} = \frac{\rho v^2}{r} \qquad \text{eq. 2.2}$$

Where **r** and **v** are the radius of curvature and velocity of the slower moving fluid within the boundary layer. As the fluid in the boundary layer moves slower than the mainstream fluid (**v<V**) it follows that it will move in a tighter radius of curvature [*Figure. 2.1*]. To counteract the overturning of the flow and preserve continuity, away from the wall a counter flow is present.

2.2.2 The boundary layer effect

The thickness of the boundary layer is a factor that affects the secondary flow in turbines. The slower moving fluid within the boundary layer introduces overturning near the end wall. Furthermore as shown by Govardhan et.al. [1986] an increase in the boundary layer thickness apart from increasing the areas of overturning near the end wall has the effect of increasing the underturning in areas away from it. However the increase in the inlet boundary layer thickness does not cause a noticeable increase in the overall loss even after the boundary layer thickness has been doubled.

In real turbomachinery the boundary layer is affected by changes in the frame of reference by moving from stator to rotor blades, and this produces a skewed flow

effect. Gregory-Smith and Walsh [1987] showed that the skew plays a significant part in the development and strength of the secondary flow by increasing the vorticity and thus the secondary flows.

2.3 Development of vortices within a blade row

The flow pattern near the end wall of a blade row is very complex and a number of flow visualization studies have aided the understanding of the physics of such flows. This includes studies by Marshal and Sieverding [1982], and flow visualization by Hodson and Dominy [1986]. An attempt to summarize the results of previous research in secondary flows was made by Sieverding [1985], which presented the secondary flow structures within turbomachinery blades. Sieverding concluded that although a good understanding of the flow structure was achieved further work was needed in understanding the significance of the various flow aspects.

Three main vortices have been identified to exist within a blade passage. These are:

- The Horseshoe vortex
- The Passage vortex
- The Counter vortex

A schematic of the structure of these three vortices can be seen in *Figure 2.2*

2.3.1 Horseshoe vortex

The end wall boundary layer upstream of a cylinder mounted on a flat plate is rolled up into a vortical motion, forming a vortex, which follows both sides of the cylinder. Due to its particular shape the vortex is termed as a horseshoe vortex.

In turbine blade rows as the blade shape is not symmetrical about the chord the two legs of the vortex are not equal. *Figure 2.3* shows the separation lines created at the stagnation point at the leading edge of the blade, caused by the horseshoe vortex where Sp is the pressure side separation line and Ss the suction side. *Figure 2.3* also shows the stagnation streamlines R and the separation saddle point A. As seen from this figure the suction side leg of the vortex keeps close to the blade and travels up the suction surface. On the other hand the pressure side leg of the horseshoe vortex crosses the blade passage and moves toward the suction surface of the adjacent blade.

3.3.2 The Passage vortex

While crossing the passage, the pressure side leg rolls up most of the inlet boundary layer which is the discharged as a loss core a small distance from the end wall (Gregory-Smith [1982]). The passage vortex rotates in the same sense as the pressure side leg of the horseshoe vortex. Squire and Winter [1951] showed that secondary flows are a consequence of the growth of a component of vorticity in the direction of the flow as it is turned around a bend. Working on the same principles Hawthorn [1955] developed a formula for the secondary circulation which when the flow

approximation is made for a flow around a bend, for a small angle θ, his formula reduces to the Squire and Winter formula (eq.2.3).

$$\Omega_s \cong -2\Omega_o\theta \qquad \textbf{eq. 2.3}$$

Where Ω_s is the secondary vorticity, Ω_o is the inlet vorticity and θ is the turning angle. The formula shows that the secondary vorticity varies almost linearly with the angle of the bend.

The passage vortex is therefore associated with the turning of the vorticity vector and dominates the later half of the blade passage. According to Marchal et.al. [1977] there is a question whether the passage vortex can be identified at the beginning from the pressure side leg of the horseshoe vortex or whether the two exist independently right from the start due to their different origin. The horseshoe vortex exists independently of the transverse pressure gradient, which is confined within the blade row, whereas the passage vortex does not theoretically need the existence of the leading edge vortex. Furthermore according to Sieverding and Van der Bosch [1983] these vortices cannot coexist separately. They combine and form a single vortex as seen in *Figure 2.4.*

Due to mutual convection by its mirror image in the end wall the vortex moves across the passage. This movement can also be associated with the strength of the vortex (Gregory-Smith and Graves [1983]). In low turning blades the movement is less compared to higher tuning blades, where the vortex based on equation 2.3 is stronger and the observed movement is higher.

2.3.3 The Counter vortex

As most of the inlet boundary layer is swept by the pressure side leg of the horseshoe vortex a new highly skewed boundary layer is formed. As the resulting cross flow meets the suction surface, a new vortex is formed close to the blade surface. The vortex has the opposite sense of rotation and thus it is called the counter vortex, or based on its location the corner vortex.

The relatively small size of the vortex compared to the passage vortex does not assist in its visualization. In cascades which are not highly loaded the detection of this vortex and measurement of the pressure difference causes proves to be difficult, as the stagnation pressure loss caused by this vortex is very small, compared to the dominating passage vortex. In highly loaded cascades the vortex caused a reduction in the overturning near the end wall region as was shown by Gregory-Smith and Graves [1983].

2.4 Flow downstream of the blade passage

The passage vortex, which dominates the blade passage, along with the counter vortex are slowly dissipated by viscous action of the fluid, some distance from the trailing edge of the blade row. However in practice the relatively small distance between two blade rows will not allow the full dissipation to take place before the flow reaches the next blade row. Additionally there is a vortex sheet shed from the

trailing edge of the blade. As discussed by Gregory-Smith [1997] in practice the vortex sheet is rolled up into one or two distinct vortices, depending on the geometry on the cascade, rotating in the opposite sense of rotation to that of the passage vortex. Furthermore according to Chen et.al. [1986] the thin boundary layer at exit from the blade passage thickens rapidly. Two peaks of loss are present downstream of the blades, one of which is closer to the end wall, whereas the other is further away from the end wall. The two peaks mix out with the blade wake and the new end wall boundary layer.

Although the magnitude of the inlet boundary layer does not significantly affect the size of the two peaks the area of high loss becomes bigger with increasing boundary layer thickness. Apart from the passage vortex and the counter vortex which dominate the flow field downstream of the blade passage, there is in addition a streamwise shed vorticity from the trailing edge of the blades. Harrison [1989] carried out experimental work on a low aspect ratio linear cascade of high turning. At 23% axial chord downstream, where one of his traversing slots was, the passage vortex was clearly visible and some of the trailing edge filament vorticity was concentrated into a discrete vortex. The two vortices coincided with the two loss peaks measured using a five hole probe.

The vortices along with the skewing produced by the interaction of the fluid between rotating and stationary parts of a turbine will considerably affect the next blade row by the unsteadiness caused at inlet.

2.5 Secondary flow calculation methods

Squire and Winter [1951] developed a technique for approximating secondary flow which was later developed by Hawthorn [1955] and Came and March [1974]. Their technique for approximation of secondary flow was to calculate the change in the component of vorticity in the direction of the flow as fluid passes round a bend.

Correlations for secondary losses derived by Dunham and Came [1970] are still widely used but contain little on the physics and is independent of blade solidity; a factor influencing end wall loss. Whereas a more recent correlation by Gregory-Smith [1982] uses "classical" secondary flow theory calculations for determining the flow angles, the loss is estimated by identifying each of its sources independently which are then added together. The physical description of the flow and the loss estimation by this method is satisfactory. However future improvement can be made by fully using three dimensional viscous flow calculations.

At Durham the definition used for the total pressure loss coefficient is usually defined as:

$$Y_S = \frac{P_{01} - P_{02}}{Q_{1MS}} \qquad \textbf{eq. 2.4}$$

The pressure P_{01} represents the free stream total pressure at inlet whereas the pressure P_{02} is the outlet spanwise average total pressure at exit. The quantity Q_{1MS} represents

the inlet dynamic pressure. The inlet dynamic pressure is used here instead of the exit because this is easily measured in the cascade.

In order to calculate the secondary loss the profile loss has to be subtracted from the total loss. The profile loss is taken as the loss at mid-span. This technique is only valid for high aspect ratio blades whereas for low aspect ratio blades a two dimensional model is used. The net secondary loss is found by subtracting the inlet loss from the gross secondary loss.

Other correlation have been reviewed by Dunham [1970] including the correlation by Hawthorn [1955]

$$Y_s = 2(\alpha_1 - \alpha_2)^2 \frac{c}{h} \frac{\cos^4 \alpha_2}{\cos^3 \alpha_m} f\left(\frac{\delta}{s \cos \alpha_2}\right) \qquad \textbf{eq. 2.5}$$

Where Y_s is the gross secondary loss based on exit dynamic pressure, c/h is a length ratio term where h is the blade height and c is the chord. In this formula the function f is a function of the boundary layer thickness δ whereas the blade turning term includes the inlet and outlet air angles relative to the blade, α_1 and α_2, as well as the vector mean angle α_m.

For most correlations, secondary loss for each blade row is a product of two terms, a loading term representing the cascade loading or turning and a length ratio term associated with the length of the secondary loss. In the review by Dunham [1970] the formula which predicted the loss most accurately was the formula derived by Ainley

and Mathienson [1952], that included the two parameters mentioned above the second of which being the function of δ_1/c.

$$Y_s = \frac{c}{h}\left(\frac{\cos a_1}{\cos \beta_1}\right)\left(\frac{C_L}{s/c}\right)^2 \frac{\cos^2 a_2}{\cos^3 a_m} \times function\left(\frac{\delta_1}{c}\right) \qquad \textbf{eq. 2.6}$$

$$Function = 0.0055 + 0.078\sqrt{\frac{\delta_1}{c}}$$

where C_L is the coefficient of lift , δ_1 the boundary layer displacement thickness and β_1 is the blade inlet angle. (all other parameters use the same notation as eq. 2.5)

More recently in their paper Chen et.al. [1986] presented a new correlation for gross secondary loss which included boundary layer velocity profile, blade loading and aspect ratio parameters. A mass-averaged inlet loss coefficient and a mass-averaged exit boundary layer coefficient were subtracted from the gross secondary loss coefficient. The formula shown below was used in order to determine the gross secondary loss

$$Y_S = Y_1 + K_1\left(\frac{C_L}{s/c}\right)^2 \frac{\cos a_2}{\cos a_1}\left(\frac{C}{h}\right) + \frac{2\delta_2/h}{(3n+1)\left(\frac{1}{2n} + 0.5 - \frac{\delta_2}{h}\right)} \qquad \textbf{eq. 2.7}$$

Where K_1=0.0055, δ_2/h=0.379(l/h) $Re^{-0.2}$, δ_2 is the exit boundary layer thickness, n is the index in the power law fitted to the boundary layer, and Y_1 is the mass-averaged inlet boundary layer loss coefficient based on exit dynamic head.

The accuracy of this formula is satisfactory as the experimental data obtained by Chen [1986] are in good agreement with the theoretical values obtained using this formula. Furthermore compared to the formula by Ainley and Mathienson [1952] Chen showed better agreement with experimental results.

2.6 Reducing secondary flows

Secondary flows can have a severe effect on turbine efficiency. The losses associated with these flows can reach up to one third and in some cases half of the overall loss. This statement shows the importance of research into ways of reducing secondary flow. As suggested by Sieverding [1975] there are several methods that can be employed to reduce secondary flow losses. These are listed here:

- Optimization of aerodynamic design
- Optimization of blade profile
- Suction or blowing
- Fences and grooves

Additionally end wall contouring is a promising method of controlling such flows.

2.6.1 Optimization of aerodynamics

Optimizing aerodynamics suggests that a careful consideration should be given to the balance between annulus area, turning angle, incidence and Mach number. Based on

research carried out by Yamamoto and Nouse [1988] in a linear turbine cascade it was established that incidence effects the three dimensional flows. An decrease in incidence would mean that the front part of the blade would become unloaded, the flow near the pressure surface could then easily separate increasing the profile loss. The secondary flow is affected by increasing incidence. The secondary loss is increased mainly due to the passage vortex, which is strengthened in the cascade due to the increase in flow turning. However at very low incidence (negative) Yamamoto et. al. [1988] reported that the passage vortex separated from the end wall moving towards mid-span whereas for higher incidence it remained fixed.

A careful consideration of incidence could assist in minimizing the secondary flow generation and therefore reduce loss. An increase in blade height would mean that the interaction between the end wall flows and the main stream flow could be minimized reducing the secondary loss coefficient. As secondary loss forms relatively close to the end wall for a blade of increased height the radial extent of the loss is relatively small and the total loss is generally smaller than for a shorter blade.

2.6.2 Optimizing blade design

Many research workers have attempted to minimize secondary flow by appropriately profiling the blade. The use of a divergent convergent blade passage was suggested by Dejc et al. [1973]. This demonstrated a reduction in the secondary losses, but at the same time an increase in the profile losses was noted. This increase was measured

when comparing the design to the conventional continuously convergent blade passage. Aft-loading of the blade can also reduce secondary flows by changing the pressure distribution around the blade. Shifting the load to the back of the blade reduces the pressure gradient at inlet that is responsible for initiating the secondary flows in the blade passage. (Hodson and Dominy [1980]).

2.6.3 Three-dimensional blade profiling

On research carried out by Dominy and Harding [1990] three-dimensional considerations of the design of nozzle guide vanes allow a significant degree of control over the distribution of total pressure losses. Dominy and Harding used blade lean to design two similar three-dimensional designs. In both designs the blade camber on the hub and at the tip was reduced, relative to a nominal mean geometry, whilst it was increased at mid-span. The reduction of the blade loading toward the tip and the hub reduces the cross passage pressure gradient resulting in reduction of the secondary loss.

In recent years the prospects of using blade lean to control the three-dimensional flows has been very promising. Lean affects the blade loading and the distribution of the loss but has a minimal effect on the overall loss. Compound lean which is stacking the blades along an arc or along a parabola, in contrast with blade lean which stacks the blades on a straight line, reduces the end wall losses (Harisson [1990]). However compound lean can also increase the mid span loss in which case there is no real gain in the overall loss. Nevertheless compound lean can be beneficial as it reduces the

mixing losses downstream and at the same time reduces the span-wise variation of the mean flow angle.

Haller [1997] investigated various methods of improving high and intermediate pressure turbine stages. Three-dimensional blade design optimization was also considered. Various 3D fixed and moving blade designs were developed in with ALSTOM and tested. Using straight tangential lean blades it was proved that the optimum stage performance depends upon the careful balance of the losses as different degrees of lean proved beneficial for a particular flow aspect whereas not for others. Compound lean was also investigated both experimentally and using CFD, and an efficiency gain of 0.4 percent was achieved. The same approach was followed for "Controlled flow" fixed blades. The "Controlled flow" is formed by skewing sections such that the throat openings are reduced at the root and increased at mid-height. This result in less mass flow passing through the end wall region where the secondary flows are generated. "Controlled flow" provides a worthwhile gain in efficiency and reduction of secondary flows. Moreover there is an area of two-dimensional flow present at mid height, in contrast with other designs.

2.6.4 Reduction by Suction and Blowing

The boundary layer at inlet to a blade is responsible for most of the secondary flows. Eliminating this boundary layer will significantly reduce the secondary flows. The most efficient way of eliminating the boundary layer is by suction. An attempt to

eliminate the boundary layer with suction was made by Gustafson [1977] using porous end walls of constant porosity. Based on conclusions from Gustafson [1977] the impact of suction was more significant on higher blade loading than at low blade loading where the influence of the side wall configuration was not measurable in terms of overall performance parameters. Prumper [1975] had previously reported that the power required to eliminate the boundary layer by suction would actually be more than the gain in efficiency.

Gregory-Smith and Besinger [1993] concluded that upstream tangential blowing into the boundary layer could reduce the loss. Although weak blowing might thicken the inlet boundary layer, with stronger blowing the counter stream-wise vorticity re-energizes the inlet boundary layer so that the passage vortex is progressively weakened. However the energy required for the inlet blowing does not leave any overall gain in the efficiency because of the mixing loss of the injected air.

2.6.5 Reduction by Boundary layer fences

Boundary layer fences have been used to correct the flow direction, which under the influence of the cross passage pressure gradients does not follow a two-dimensional flow pattern. The fences are meant to reduce the radial extent of the secondary flows and reduce the mixing losses by reducing the interaction of the boundary layers with different flow directions. Prumper [1975] suggested that fences can be applied to

either the suction surface or the pressure surface independently or to both simultaneously and on the end wall.

Kawai et.al. [1989] showed that fences attached to the end walls within the blade passage of a linear turbine rotor cascade are capable of reducing both secondary flows and total pressure loss. Furthermore a conclusion on the most effective height of the fences was reached which is one third of the inlet boundary layer thickness and located half a blade pitch away from the blades. With this arrangement the passage vortex and secondary vorticity region are reduced, moreover the secondary kinetic energy and the maximum underturning are reduced by half.

However the application of boundary layer fences to real turbomachinery is questionable, as metal fences have to be strong enough to withstand the forces applied and to operate at an elevated temperature.

2.7 End wall profiling

Early research on secondary flow reduction by means of end wall contouring was carried out in the 1960's and continues until the present day. The most common test configuration of end wall profiling in turbine cascades is having one planar end wall and the other profiled.

Deich [1960] identified that to achieve further improvements in efficiency is scarcely feasible as modern cascades had already achieved minimal profile losses, which depend on the reaction. It was suggested that substantial increase could be achieved by using special profiling of the end wall. The effects of this method could be more noticeable in guide vane cascades as the entropy change in a nozzle row is higher than in a rotor blade row. Furthermore as presented in *Figure 2.5* the exit dynamic head and therefore the velocity $\mathbf{V_2}$ is higher for a nozzle row, represented as process 1-2, than for a rotor blade row where the exit relative velocity $\mathbf{W_3}$, which would be measured in a cascade is lower. Therefore the same of loss coefficient is more significant for a turbine nozzle row than for a rotor blade row, as quantitatively the loss is more. Deich [1960] selected profiles that reduced the velocity in the regions of highest turning and provided increased acceleration of the flow just upstream of the trailing edge. The use of non-symmetrical end wall profiling produced a sharp reduction in the end losses and an equalization of the velocity field behind the cascade. An absolute increase in efficiency in the order of 3.0-3.5 per cent was reported for very low aspect ratio (0.5) blades.

Morris et. al. [1975] carried out experimental work on a linear cascade testing several forms of end wall profiling with varying aspect ratio and inlet boundary layer thickness as it was believed that the blade height and boundary layer thickness reported by Deich [1960] was unrealistically low. Four different profiles were tested. The profiles were reported to reduce fluid velocity over the front portion of the blade where turning is higher and a reduction in loss was achieved. Although the profile presented a beneficial effect in the front of the blade an increase in the adverse

pressure gradients over the rear of the blades' suction surface was noted. The symmetric cubic end wall profile within the blade passage showed a reduction of 25 percent in the secondary loss for an aspect ratio of 0.5, which decreased with increasing aspect ratio. The reduction in losses was observed near the planar end wall and were caused by the redistribution of the pressure due to profiling. However profiling upstream of the blade passage did not have any effect on the losses.

Walterman et. al. [1976] conducted a series of experimental tests on three low aspect ratio cascades, two of which had one of the end walls profiled whereas one of the cascades used blades designed for more uniform turning rate and increased trailing edge wedge angle. Influence of the tip loading and minor changes at the mid-span section were reported. The maximum suction surface velocity was shifted rearward. Apparently the effect of the end wall contouring was to radially redistribute the losses but it did not significantly change the mass-average loss level.

Kopper and Millano [1980] experimented on two linear cascades. The two cascades shared the same blade type. One of the cascades had one of the end walls profiled in the axial direction keeping the second planar whereas the second cascade had both end walls planar. Comparing data from the two cascades, the profiled end wall was more lightly loaded suggesting improvements in the performance of that cascade. In the profiled end wall cascade a reduction in the cross passage pressure gradient was also achieved. Moreover the profiled end wall cascade demonstrated a 17 percent reduction of the passage mass-averaged loss and a reduction of the secondary loss near the planar end wall side of the cascade.

Atkins [1987] was the first to identify the need of a systematic way to design and select end wall profiles. Using a computer three-dimensional calculation program the effect of a particular end wall geometry on the pressure distribution on the blade and on the end wall could be predicted. Different designs could then be tested before manufacture, and the ones that produced the more desirable properties were manufactured and tested. Seven different geometries were manufactured and tested. Out of the seven profiles the one pictured in *Figure 2.6* proved to produce the best results as the aerodynamic blade loading near the end wall was reduced resulting in a lower cross-passage pressure gradient. This in turn reduced the amount of low energy fluid that was swept from the end wall boundary layer away from the end wall and into the passage vortex. In the concluding remarks of Atkin's paper the need of a method to iteratively design an end wall with a prescribed pressure distribution was stressed and that a useful application of such a design could help in significantly reducing secondary losses was also pointed out.

More recently other researchers had taken this approach. Duden [1998] tested a highly loaded cascade with three-dimensional end wall contouring after a 3D-computer design environment systematic study. The resulting end wall and 3D designed blades demonstrated improvements concerning the radial extent of the secondary flow. A decrease in the secondary loss of 16 percent was reported only to be counterbalanced by increased profile losses and higher inlet losses due to increased blockage. However the exit flow angle deviations was reduced giving a more uniform flow entering the next blade row.

Hartland et. al. [1998] produced a non-axisymetric end wall profile using CFD as a design tool which was fitted to a large scale linear turbine rotor blades cascade. The research was based on previous work by Rose [1994]. The profile was based on the assumption that the end wall static pressure can be locally raised or lowered by applying curvature to the end wall. The design of such a profile aided in the conclusion that three-dimensional design similar to that used for blades can be used for end walls so that a desirable pressure distribution can be achieved which could result in secondary flow reduction. Moreover Hartland concluded that further appreciation of the flow physics is required in order to develop more successful designs. Hartland et.al [1999] applied this method in design of a non-axisymmetric profile which reduced secondary flows as well as secondary kinetic energy and exit angle variation.

The work carried out by Yan et. al. [1999c] and the author can be regarded as a further step to the research presented in this section, as a systematic CDF testing was carried out before producing a non-axisymetric design which demonstrated a reduction of secondary loss and less angle variation. Yan et. al. [1999a] using CFD produced and tested four groups of profiles. The stream-wise profile was designed based on the assumption that the end wall static pressure can be raised locally by applying a concave curvature and similarly lowered by applying a convex. Based on previous work by Deich, Yan chose profiles that reduced the velocity in the region of highest turning and provided increased acceleration of the flow just upstream of the trailing edge. A similar profile was applied in the tangential direction. The upstream

and downstream shapes of the blade passage were not altered and profiling was constrained within the blade row, thus making feasible the application of this design to real turbomachinery. The parameters used for the axial design are the distance between the trailing edge and the peak of the axial profile (ct), the amplitude of peak (2xat) (*Figure 2.7*) whereas in the tangential direction a sinusoidal profile was originally used. After a detailed CFD investigation of the four types the best profile was selected and manufactured. The final profile, in the tangential direction, instead of a fully sinusoidal curve used a sinusoid close to the suction surface and close to the pressure surface the end wall was kept flat (*Figure 2.8*). Yan carried out a series of experiments for both planar and profiled end wall and showed that the profile reduced the secondary losses by 23% and secondary kinetic energy which was reduced by 24%, whereas no significant effect was measured in exit yaw angle.

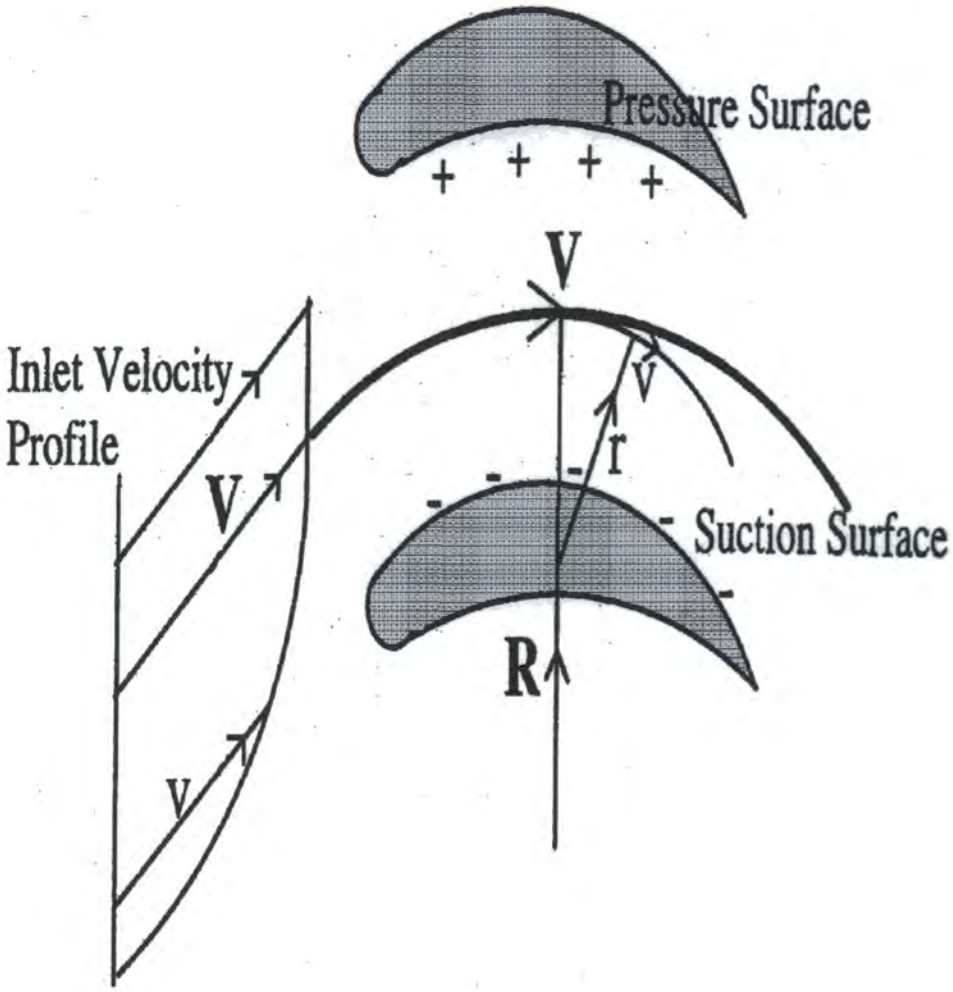

Figure 2.1: Cross passage pressure and velocity gradient

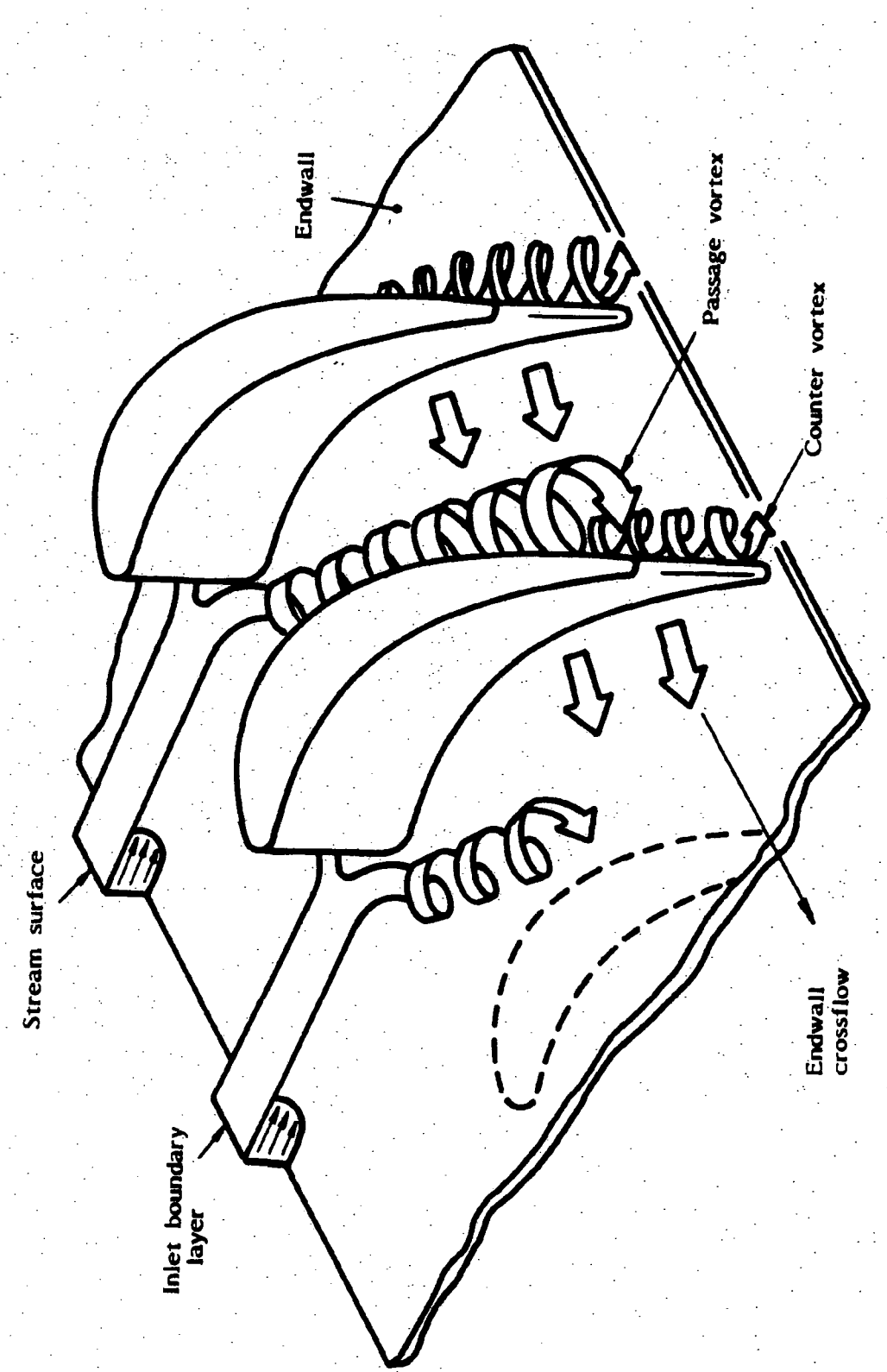

Figure 2.2: Secondary flow vortices

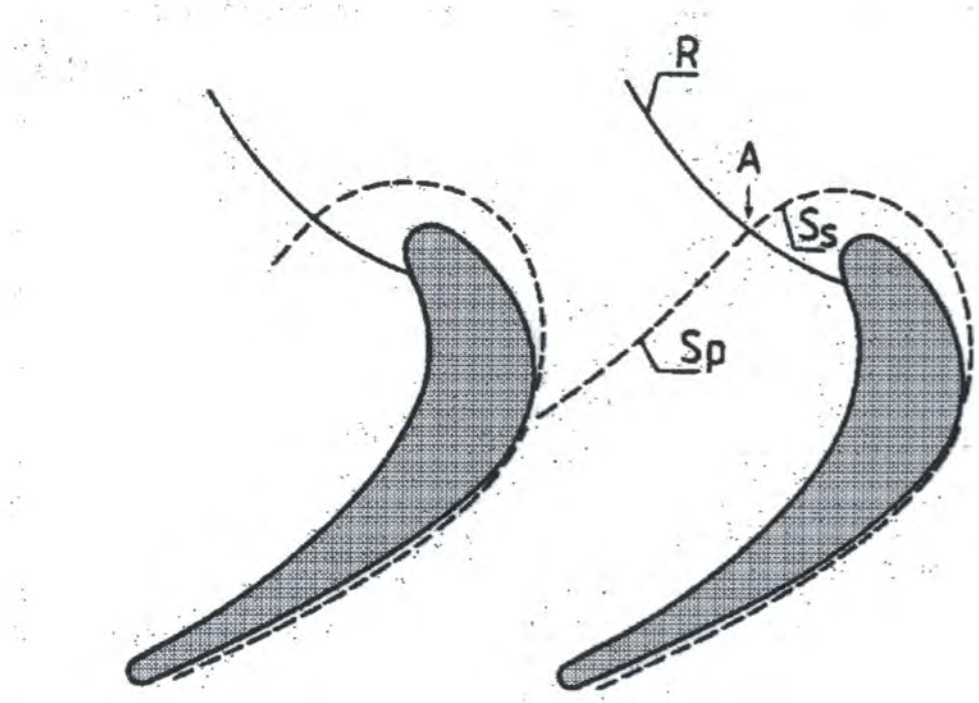

Figure 2.3: Flow separation lines

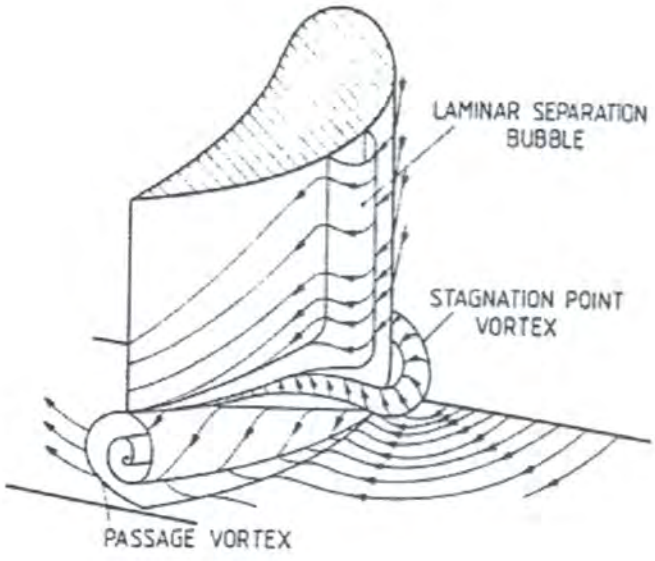

Figure 2.4: The passage vortex

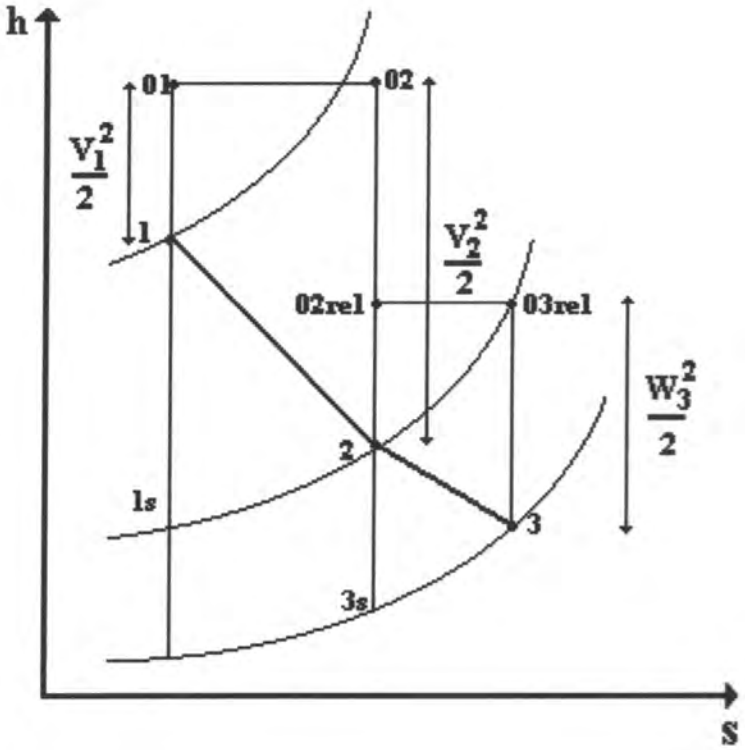

Figure 2.5: Turbine stage

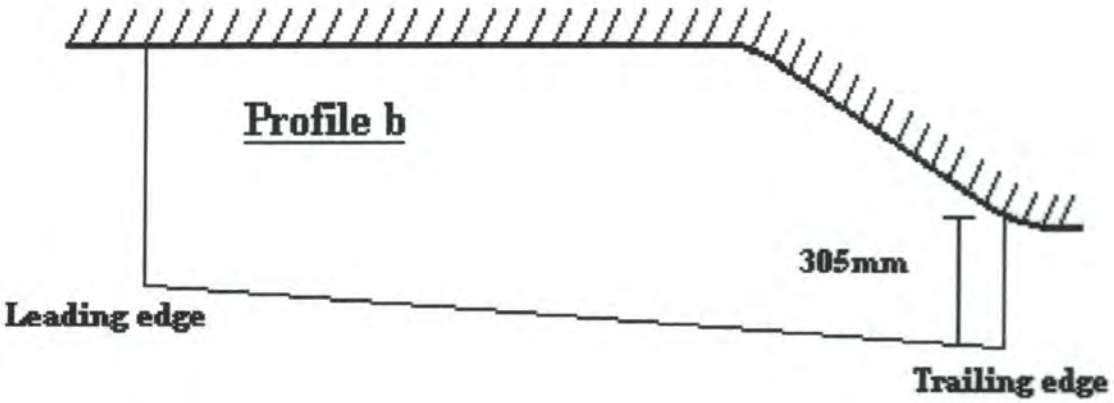

Figure 2.6: Atkins' [1987] end wall profile

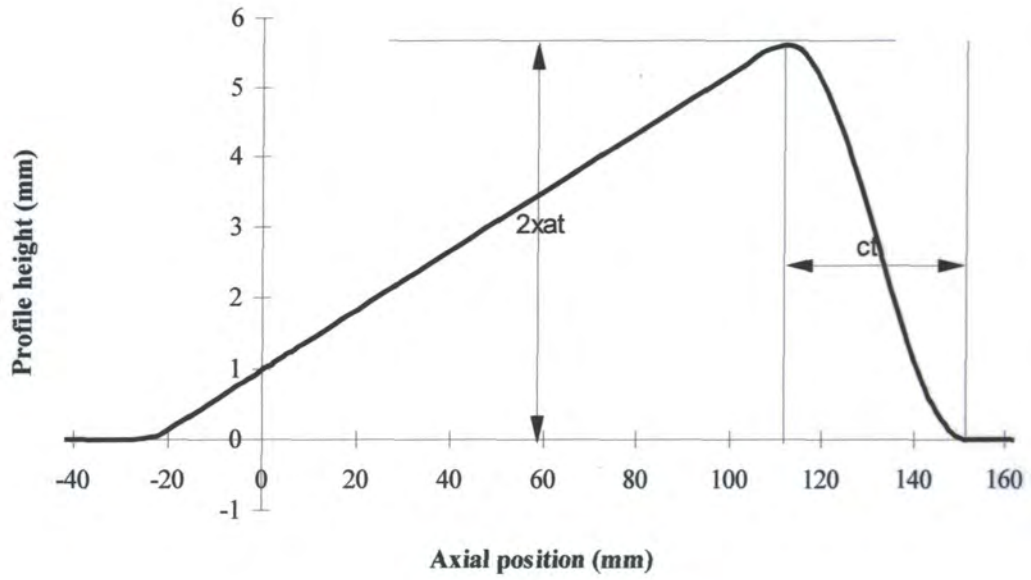

Figure 2.7: The end wall shape in the axial direction

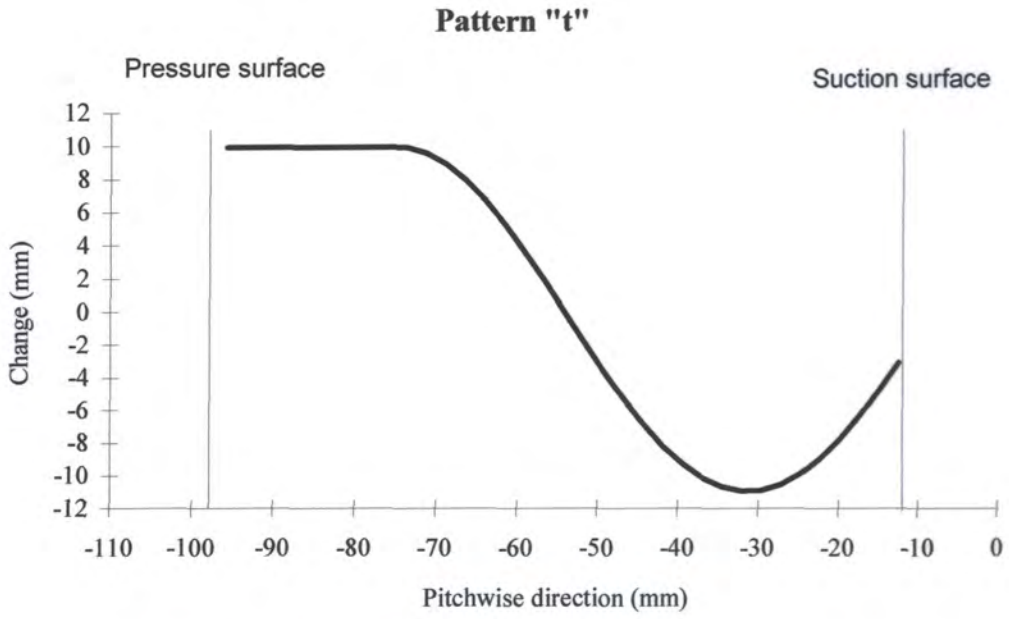

Figure 2.8: The end wall shape in the tangential direction

Chapter 3

Experimental apparatus

The apparatus used can be divided into two main categories. These two main sections are:

a) The cascade, which includes the blades, based on the ALSTOM Energy model, and the turbulence generation grid
b) The traverse gear and data acquisition, including probes and calibration equipment.

Attention has been given to the periodicity and the accuracy of the results. Several features have been incorporated to maintain the highest degree of accuracy possible. The use of tailboards and boundary layer control gaps are some of the features used.

3.1 The Cascade

The cascade is a linear model with air being blown through a single turbine nozzle blade row. The air supply is given by a large, low speed, blowing wind tunnel. A variable speed motor drives a Blackman series 28, double entry, centrifugal fan, which is used for blowing. The air leaving the fan passes through parallel wall section, a diffuser and reaches a large settling chamber, at the end of which a contraction section accelerates the flow. The accelerated flow needs to be uniform, so a honeycomb flow straightener is used in the settling chamber.

The flow leaving this part of the wind tunnel enters the main section of the cascade through a turbulence generation grid. The grid is used in order to achieve a more realistic turbulence intensity, as the free stream turbulence of a cascade in most wind tunnels is far less than real in turbomachinery.

3.1.1 Turbulence generation grid and false side wall

Low turbulence intensity would mean that some regions around the blade could sustain laminar flow. In a real turbine nozzle blade row this region would not exist, as the turbulence intensity and Reynolds number would be much higher, therefore its elimination is deemed necessary in order to achieve a more realistic flow field. Furthermore, laminar regions on the suction surface could give rise to separation bubbles, thus extra loss would be present which under normal operating conditions would not be present in a real turbomachine. The grid aims to minimise these areas and achieve a fully turbulent flow.

The grid (designed by Yan [1999]), uses 25mm diameter metal bars both in the horizontal and vertical directions. Whereas the horizontal bars are placed at a fixed interval of 100mm apart), the vertical bars where designed to be adjustable so that the required boundary layer profile *(Figure 3.1)*, at inlet to the blade row, could be achieved.

Previous research has shown that in order to achieve a satisfactory boundary layer profile at inlet an extra bar of smaller diameter has to be used. Investigations carried out on the velocity profile at inlet revealed the existence of a small bump near the end wall region, resulting from a wider gap between the last vertical bar of the turbulence grid and the end wall. A small half-inch bar was fitted 24mm from the side wall between the last bar and the end wall, which eliminated this abnormality in the velocity profile.

The turbulence intensity level achieved by this method is approximately 5% at inlet whereas at 75% of the axial chord upstream of the blade row, the intensity in the

stream wise direction is 5.4% according to Yan [1999]. After a series of tests had been carried out, a separation bubble was still present on the suction surface of the blades. This was dealt with by placing a transition trip along the span of blade over the suction surface, which produced a fully turbulent flow.

The flow leaving the Durham wind tunnel exits from a section of 700mm height and 460mm width. The same dimensions are used for the casing of the turbulence generation grid, and the false sidewall whose length is 800mm for easier connection to the wind tunnel (*Figure 3.2*). The test section dimensions are 700mm by 400mm leaving a gap of 60mm. The flow from this gap can bleed off the upstream boundary layer. A bracket was mounted near the leading edge of the false sidewall in order to obtain equal pressure at both sides of the leading edge. Details of this feature can be seen in *Figure 3.2*. The arrangement of the turbulence grid and the bracket was kept the same as that followed by Yan [1999] for his experiments, as the series of tests carried out are a continuation of his work.

3.1.2 The arrangement and the number of blades.

The blades used for the test section of the cascade are based on the ALSTOM turbine nozzle blades. Details of the blades can be seen in the first row of *Table 3.1,* below.

	Axial chord (c_{ax}), mm	Chord (c), mm	Pitch (s), mm	Inlet Angle	Outlet Angle	Throat Mm
Full size blade	92.55	136.54	85.09	0	77	20
Cascade blade	152.28	224.65	140	0	77	32.94

Table 3.1 – Blades

Using the blade provided by ALSTOM would make use of pressure probes difficult as the space for moving the probe within the passage would be limited. Furthermore the blockage caused by a probe within a small blade passage would affect the flow

considerably more than the same probe being used in a larger scale model of the same cascade. This would mean that additional loss would be present depending on the relative size of the probe compared with the blade geometry, and size. Thus the blade described in the first row of *Table 3.1* was used as a model for building a larger scale equivalent shown in the second row of the same table, increasing the throat width by approximately 13mm.

Six of the blades described above were used for the cascade, which provided a sufficient number of passages for periodicity purposes. They provide five passages out of which the middle one was used for gathering experimental data and running tests, which gave the acceptable results in terms of periodicity.

The two outer blades have a span of 400mm whereas the four inner blades are 20mm longer as they are manufactured so that 5% of the length fits into the end wall under investigation. All six blades were cast in epoxy resin according to a metal master blade provided by ALSTOM. The suction side and the pressure side of the two blades in the central passage were fitted with static pressure tappings, manufactured by hypodermic tubing being cast in the blade. The pressure tappings were not used during these series of tests so they were sealed using a thin plastic tape.

3.1.3 End wall window and traversing planes

The cascade as designed by Yan [1999] can be seen in *Figure 3.3*. The test section has an overall height of 1130mm whereas the shorter edge is 990mm. The axial width of the cascade is 320mm. Ten slots are cut out of one side wall allowing traversing in two different planes upstream of the blade, one vertical and one horizontal, which is used for obtaining the velocity profile upstream of the blade passage. There are six slots covering the blade passage allowing measurements to be taken over the whole span and two more traversing slots downstream of the blades. The last two slots were used for the purposes of this research (*Figure 3.4*). Details of the slot positioning are given in the following table (*Table 3.2*)

Slot	1	2	3	4	5	6	7	8	9	10
X/C_{ax}(%)	-75	-13	3.3	25	50	70	85	97	113	126

Table 3.2 – Traversing planes

The origin for co-ordinates of the cascade is the trailing edge of the lower blade. Co-ordinates are taken assuming the origin is the trailing edge of the lower testing blade on the surface of the end wall and positive span-wise direction is moving away from the end wall. Slots nine and ten, which are used for testing have a length of 250mm covering the wake of the two blades in the central passage. All slots when not in use are sealed with a T-shaped wood filler manufactured to fit exactly each hole to ensure no air leaks and that the end wall surface is as smooth as possible. The traversing slot in use is sealed using a rubber seal, which is lubricated, or a brush type seal. This allows the probe to move freely in that plane but at the same time prevents most of the flow from leaking through that opening.

The end wall under investigation is fitted on the opposite side of the cascade to the slotted end wall on a window 500mm by 230mm that is cut out of the cascade wall. This arrangement allows different end wall regions to be fitted and investigated. The tests carried out involve only one design of profiled end wall and the flat end wall. The flat end wall is manufactured by using a CNC machine to cut a Perspex glass the size of the window. The use of Perspex was necessary as previous research included flow visualisation. The end wall was also fitted with static pressure tappings. The hypodermic tubing used for the tappings was blocked during the series of experiments making sure that no flow leaked through.

3.2 Data acquisition and traverse gear

The data acquisition equipment include a series of pressure probes and pressure transducers along with a PC – 386DX and a set of programs written in C. There are

two probes used at any given time. A pitot static probe is used to measure the characteristics of the flow upstream of the blade passage and the second probe used for traversing.

3.2.1 Probes

A pitot static probe is installed upstream of the blades and used as a reference for all the other pressures measured by other probes. It is installed 700mm upstream of the leading edge and measures total pressure and static which are then transferred to the computer

The experiments carried out and presented by Yan [1999] were based on a 5-hole cobra probe designed and manufactured in the university of Durham (*Figure 3.5*). The probe was calibrated by the same method as that of Treaster and Yocum (1979). The calibration was carried out at a high dynamic pressure close to the exit dynamic pressure of the cascade, which gave a smooth calibration map, although there was not a noticeable difference between the lower dynamic pressure calibrations. For calibration purposes a variable speed air pump was used which was connected via a flexible pipe to a cylindrical duct which had a honeycomb flow straightener fitted. The probe was connected via hypodermic tubing to a scanivalve, which was then connected to two transducers. The calibration was automated by using a computer to drive two stepper motors, which controlled the movement of the probe in the pitch and yaw direction.

This series of experiments carried out used a similar probe to the one described above, the only difference being that the probe had smaller outside dimensions, which allowed measurements to be taken closer to the end wall and at the same time causing less blockage to the flow. The hypodermic tubing used for this probe (designed by Hartland [1998]) had the same internal diameters and approximately the same length as Yan's probe.

As there was need for a closer investigation of the flow near the end wall region a new probe was designed and manufactured. The probe is a flattened pitot probe that allows measurements to be taken starting from 0.3mm from the end wall (*Figure.3.6*) An investigation of the sensitivity of the probe to yaw angle variation was carried out. It was shown that the probe could accurately record the total pressure of a moving fluid within a band of 10 to 15 degrees, 5 to 7 degrees both for the positive and negative yaw angle. The total pressure measurement by the probe was compared to the reading of a pitot static probe facing the flow at zero angle. The difference between the two probes was then non-dimensionalised by dividing by the dynamic head. Assuming that the yaw angle deviation is small, the difference between the actual and the measured total pressure caused by the difference in angle setting should be negligible so the probe accuracy was high. This can be seen from *Figure 3.7*. As some instability was present in the flow the bottom part of the graph is not entirely smooth and two points between 0 and 5 degrees do not give a near zero value, which is believed to be due to experimental error.

3.2.2 Transducers

The probes used are connected by means of PVC tubing to pressure transducers. The five-hole probe arrangement uses four CMR CONTROLS 200-013 P-sensor transducers able to measure positive pressure differences up to 2000Pa giving a 0–5V linear output. One side of these transducers is connected to one of the four side holes of the five-hole probe, the other side is referenced back to the upstream total pressure measured by the pitot static probe. The total pressure measured by the central hole of the five-hole probe is connected to one side of a transducer, with a range of ±200Pa whereas the other side is again connected to the upstream total pressure. Finally this arrangement uses a transducer capable of reading positive pressure differences up to 500Pa to record the difference between total and static pressure measured by the pitot static probe. A connection map of this arrangement can be seen in *Figure 3.8*. The ±200Pa transducer is used for the flattened pitot arrangement. The four 0-2000Pa transducers are not used and the only other active transducer is the one connected to

the pitot static probe upstream, so the arrangement is simplified to the one shown in *Figure 3.9.* All the transducers used are pre-calibrated by the manufacturers but the calibrations were checked during the testing and little or no deviation was found. The transducers are connected to an analogue to digital converter, which has a 12-bit resolution and takes ±5V input. A standard card samples 16 channels at speeds of up to 30 kHz. Only six are used when testing with the five hole probe, one for each hole of the probe and one for the pitot static probe reading, whereas only two channels are used when testing with the flattened pitot probe.

3.2.3 Traverse gear

The probes used for data acquisition are mounted on the traverse gear provided by Time and Precision Ltd. Two A4012Q1 unislides are used 304 mm in length. These two slides control the tangential and radial movement of the probe and a rotary table mounted on one of the two unislides controls the angular movement of the probe. The layout of slides is shown in *Figure 3.10.* Fitted to the end of each slide, there is a 400 half steps per revolution stepper motor. The step of the motor is 1.8°, which gives a resolution of 0.005 mm. The Time and Precision A375TS rotary table that holds the probe is driven by a 200 step per revolution step motor with a 90:1 gear ratio, which gives an angular resolution of 0.02 degrees. A 4-phase bipolar driver board (RS 342-501) drives every motor. The driver board is controlled by a 48-channel input / output board installed in the PC – 386DX computer.

3.2.4 Software

There are three main categories of software used; the main set of programs for controlling the movement of the probe and traverse gear along with the data acquisition, the analysis software, and the graph plotting software.

Traversing and data acquisition is controlled by a series of programs first developed by Biesieger (1993) and also used by Yan [1999]. The programs are written in C, and control both the traversing and the data collection. A grid file is used to indicate the co-ordinates of the data collection points, and data are collected over a period of ten seconds. Due to fluctuations in the flow this time was necessary to achieve an accurate average value. The computer averages the data collected and all values are referred back to standard day conditions shown in *Table 3.3*.

Atmospheric Temperature °C	Atmospheric Pressure mm Hg	Air Viscosity mPa s
17	776	$1.5\ 10^{-5}$

Table 3.3 - Standard day conditions

The data acquisition is performed on a constant Reynolds number basis to ensure consistency of the results. The dynamic head is calculated and displayed on the screen after the atmospheric conditions have been inserted to the program. Once the required dynamic head has been achieved by controlling the speed of the wind tunnel the program refers to the grid file for the data collection. The probe is always traversed away from the end wall, and is set at the flow angle that corresponds to the mid-span flow angle. This information is also included in the grid file. After each point the information collected from the probes is stored in a file which also includes the atmospheric conditions and the dynamic head.

The file obtained by a five-hole probe traverse can then be transferred to a UNIX terminal and is analysed by a program written in FORTRAN. This allows the calibration map to be applied to the results obtaining pitch and yaw angle, total and static pressure, for every set of tangential and radial co-ordinates.

This procedure was followed by Yan [1999] for the sets his data presented in this thesis. Due to transducer discrepancies the same procedure could not be followed for obtaining the yaw angle for the experiments carried out with the five-hole probe. The yaw angle was instead measured manually, using a U-shaped manometer. The two

ends of the manometer was connected to each of the five hole probe tube that corresponded to yaw angle. The manometer setting was such that at mid span and mid pitch the pressure was equal in the two tubes. The probe was then traversed over the grid, adjusting the angle so that any pressure difference between the two tubes would be eliminated. The new yaw angle was then read from the rotary table. This method was only followed as an alternative due to the possible fault of the transducers, as it is not expected to be as accurate as the one used by Yan. Further analysis of the results was then carried out using a modified version of a spreadsheet developed by Hartland. When testing is carried out with the flattened pitot probe the results do not have to be referred to any calibration map, so this step was not followed for the analysis.

Once the results have been analysed they are plotted using a series of graph plotting software both in UNIX and in Windows environment. Two of the most frequently used packages are Microsoft Excel for Windows and Sigma Plot. From the results the total pressure loss coefficient and static pressure coefficient are obtained. The total pressure loss coefficients are used for area contour plots and are pitch averaged across a wake thus obtaining the pitch averaged coefficients which are plotted using Excel. The flattened pitot pitch averaged results are obtained by using the total pressure and yaw angle measured with the five hole probe in conjunction with the flattened pitot data, where the two traverse grids agreed. Whereas closer to the end wall pitch averaged values were obtained by extrapolating the angles and static pressure coefficients, using the existing data. The yaw angle is also pitch averaged over the half-span area and plotted using Excel whereas area contour plots of yaw angle are produced using Sigma Plot. All pitch averaging is carried out across a wake in contrast with Yan's approach to pitch average between the two wake peaks.

Data from Yan and the five hole probe are also area mass-averaged. Area averaging is also carried out using a mixed data approach. For a more accurate estimation of the secondary loss, data from the flattened pitot probe for the area close to the end wall are used in conjunction with the five hole probe data from 10mm outwards to produce the mixed data area averaged values. The definitions of the coefficients are shown in the Appendix.

3.3. Experimental accuracy.

The accuracy of the experiments depended on several factors regarding the sensitivity of the equipment, the error in positioning and the stability of the flow. These factors are presented here in order for their contribution to the final measurement to be quantified.

3.3.1 Positioning error

All measurements have been carried out with either of the two probes (*Figure 3.5, Figure 3.6)* mounted on the traverse gear. The stem of the probe fits exactly on the traverse gear allowing little deflection by the flow in the front part of the probes due to their small thickness. The five-hole probe deflection was in the order of 0.1mm, and the error in its initial positioning was between 0.1 to 0.5mm. Due to its less rigid construction the deflection of the flattened pitot probe was within 0.5mm, whereas the positional error of this probe was of the same magnitude as the five-hole probe. The error caused by the initial positioning of the traverse gear in conjunction with the stepper motor error was within 0.5mm.

3.3.2. Probe accuracy.

The five-hole probe calibration was accurate for flow angles that did not exceed 25° whereas the error was within ± 1% of the total pressure loss coefficient. The flattened pitot probe could accurately measure the total pressure loss coefficient within a range of angle of ± 5°. In this region the error would be less than ± 0.001 of the CP_o value.

The pitot static probe, which was used to measure the upstream dynamic head, was set to the inlet flow angle by using a micro-manometer. (Setting the probe to the angle of the maximum dynamic head ensured that it was set at the inlet angle).

3.3.3. Upstream velocity.

The computer program measured the dynamic head continuously. Although there was some fluctuation of the air speed the value of the dynamic head was measured over a period of 10 seconds at each grid point traversed and was then averaged, thus eliminating the error due to the fluctuations. For better accuracy, instead of a single value for the dynamic head, the averaged value at each grid point was used.

3.3.4 Manual yaw angle measurement.

The yaw angle was measured manually with the five-hole probe. Using a micromanometer and the angle dial that the probe was mounted on, an accuracy of $\pm 0.1^{\circ}$ could be achieved. An initial positioning error of the same magnitude could be expected when setting the probe to the mid-span flow angle before each traverse.

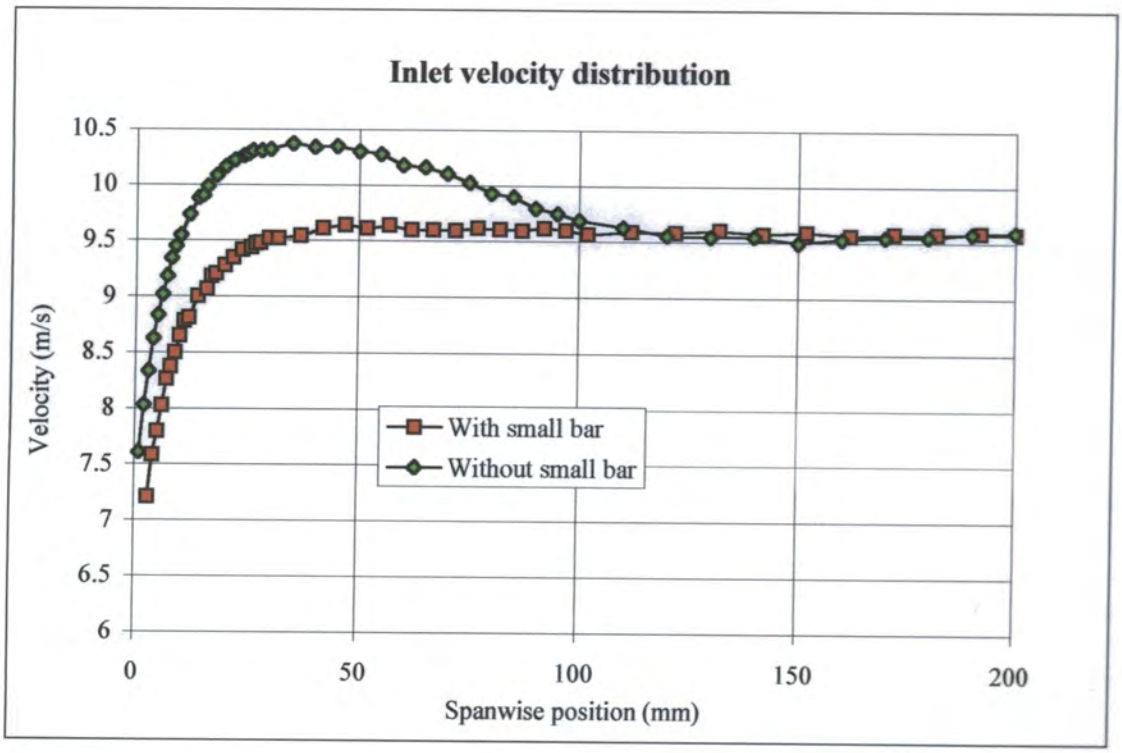

Figure 3.1 Inlet boundary layer

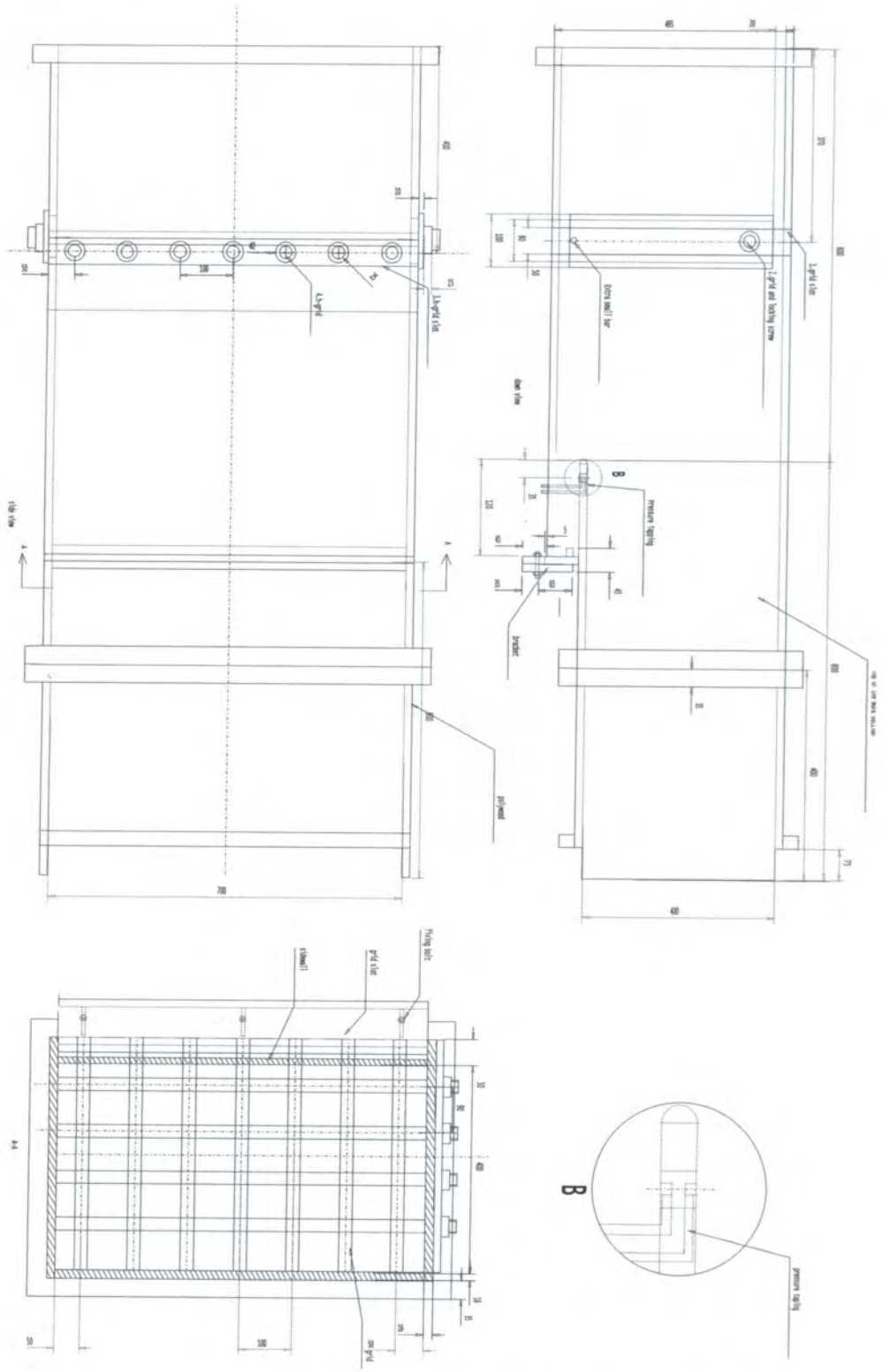

Figure 3.2: Cascade and turbulence generation grid

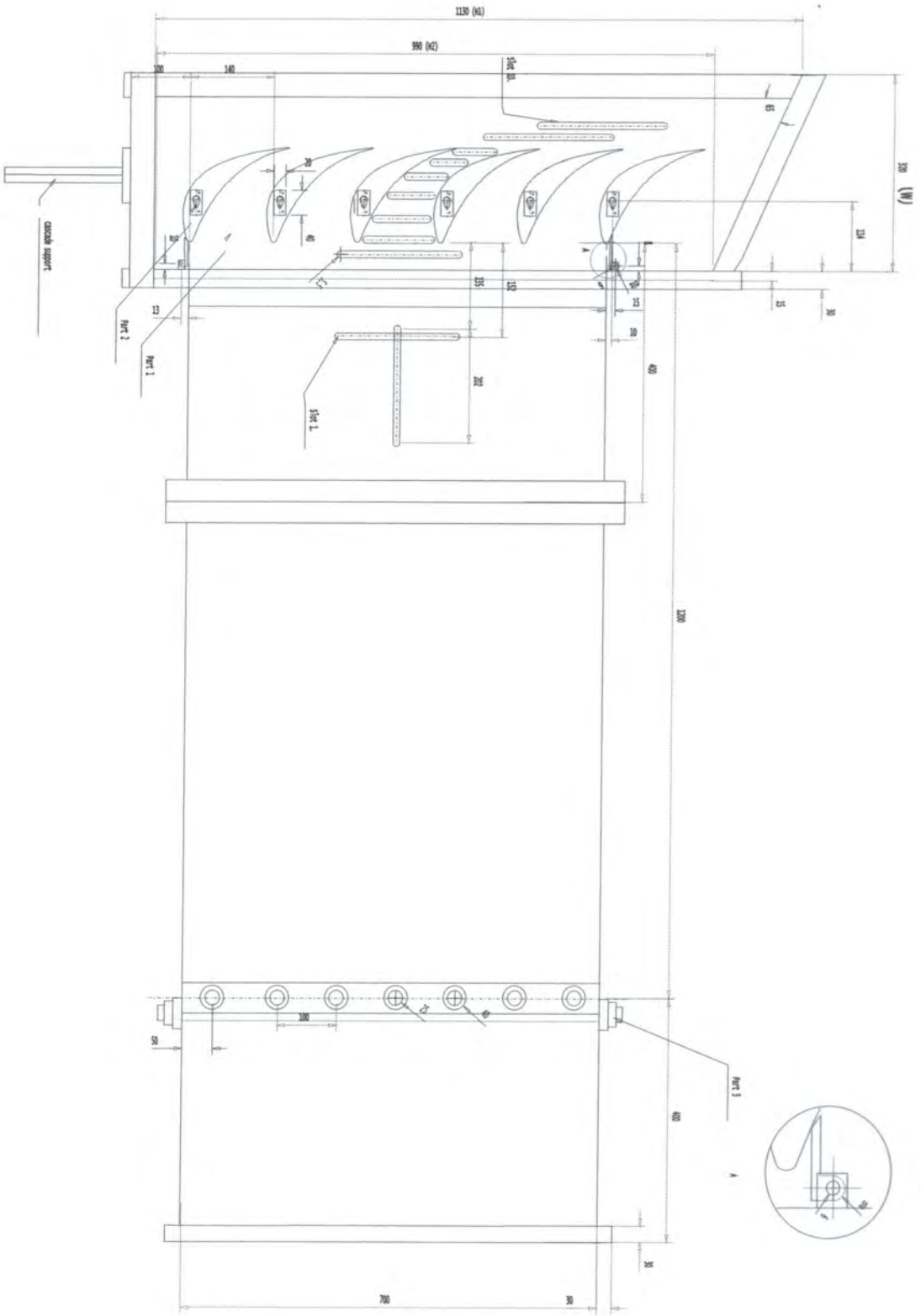

Figure 3.3 Cascade and test section

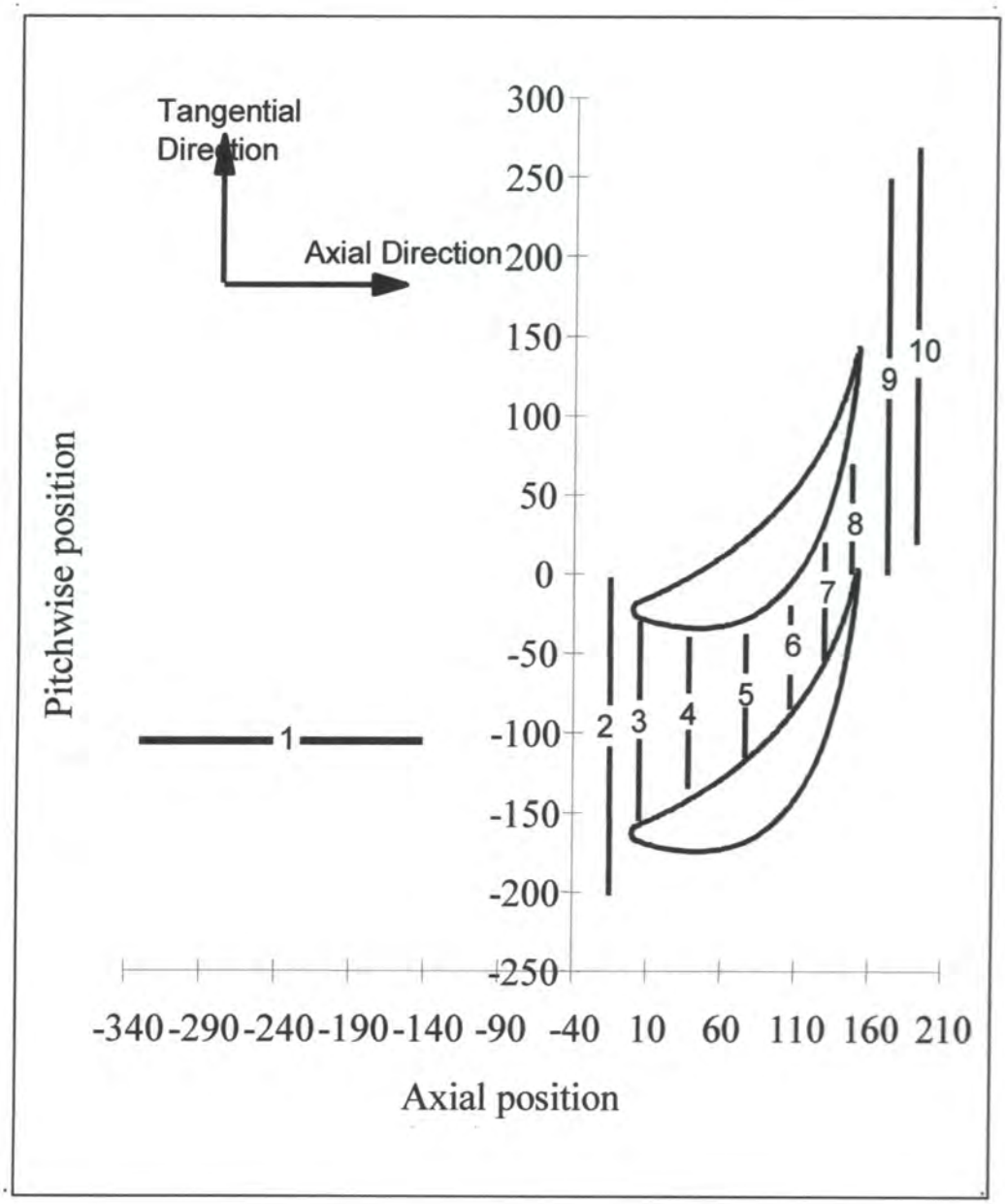

Figure 3.4: Slot positions

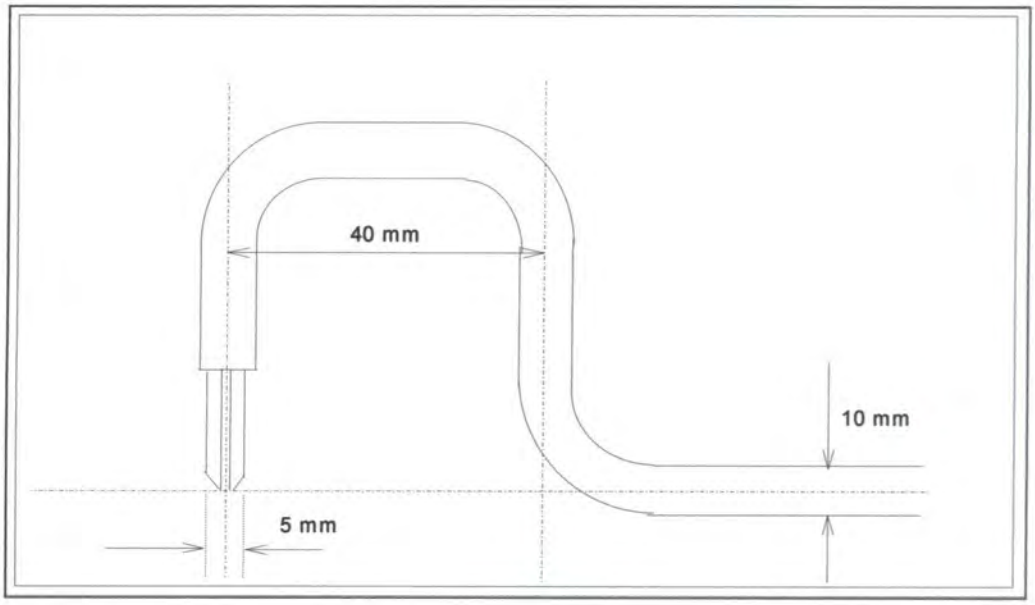

Figure 3.5: Cobra probe

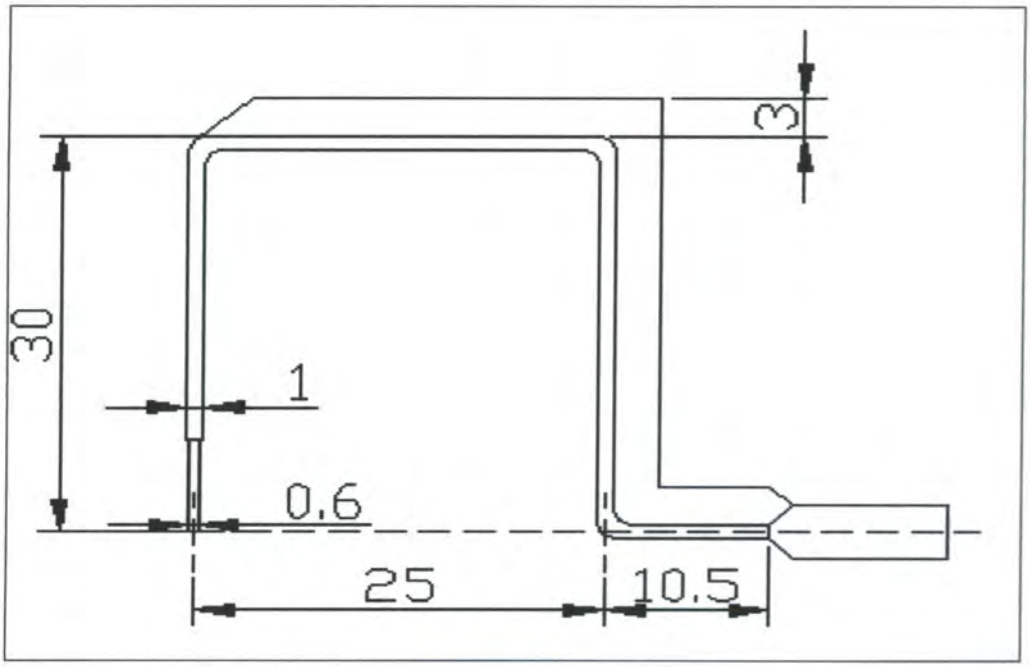

Figure 3.6: Flattened pitot probe

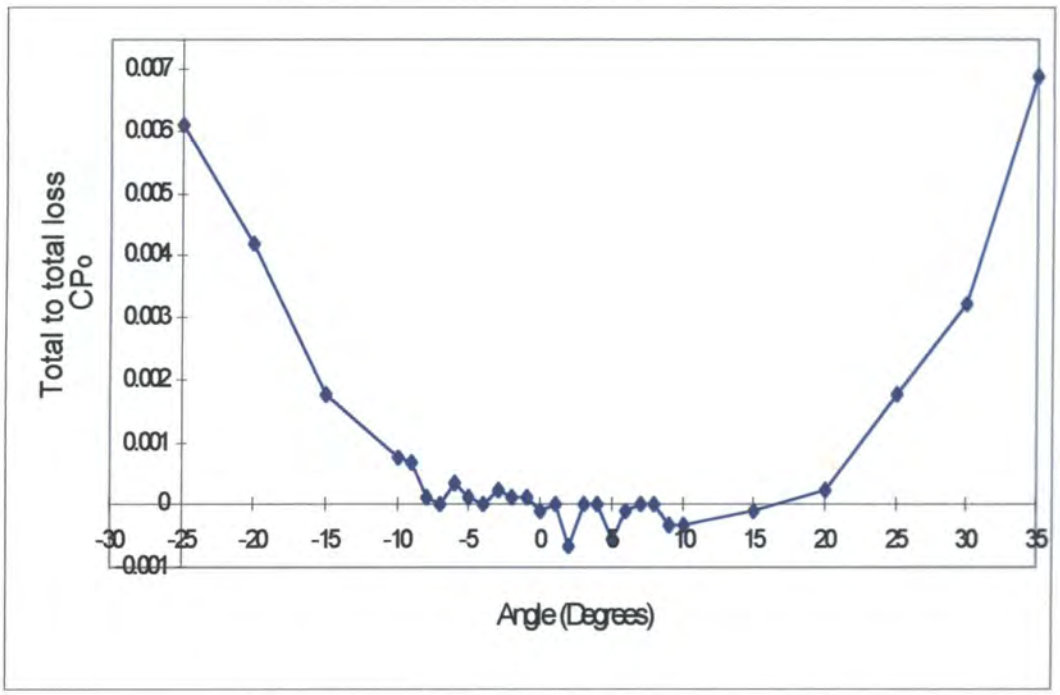

Figure 3.7 - Flattened Pitot Probe Angle Sensitivity

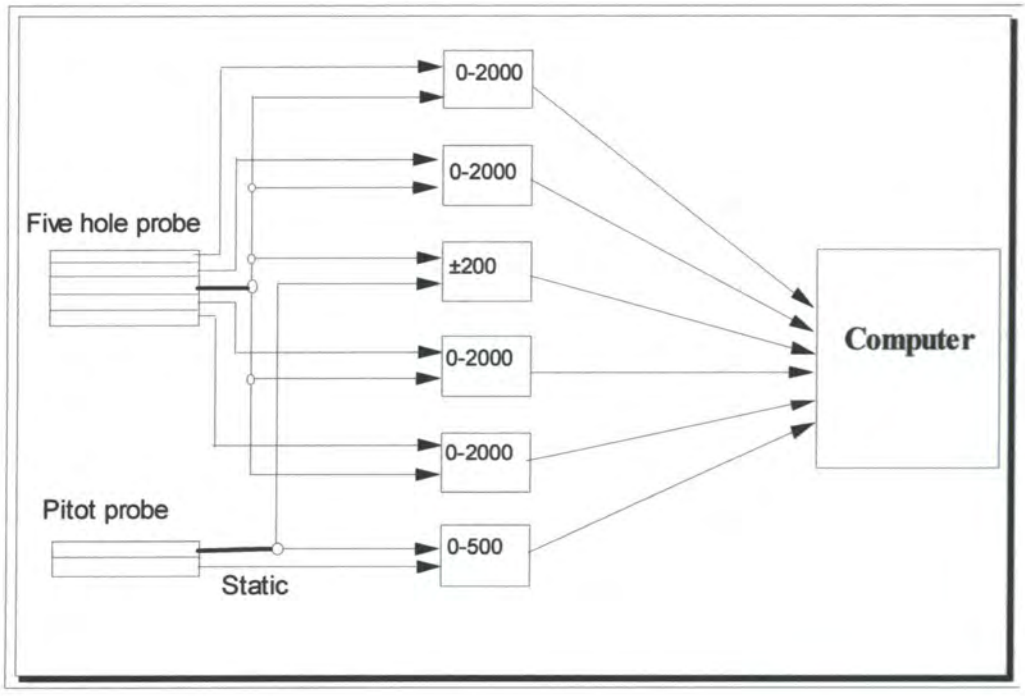

Figure 3.8: Five hole probe transducer arrangement Yan [1999]

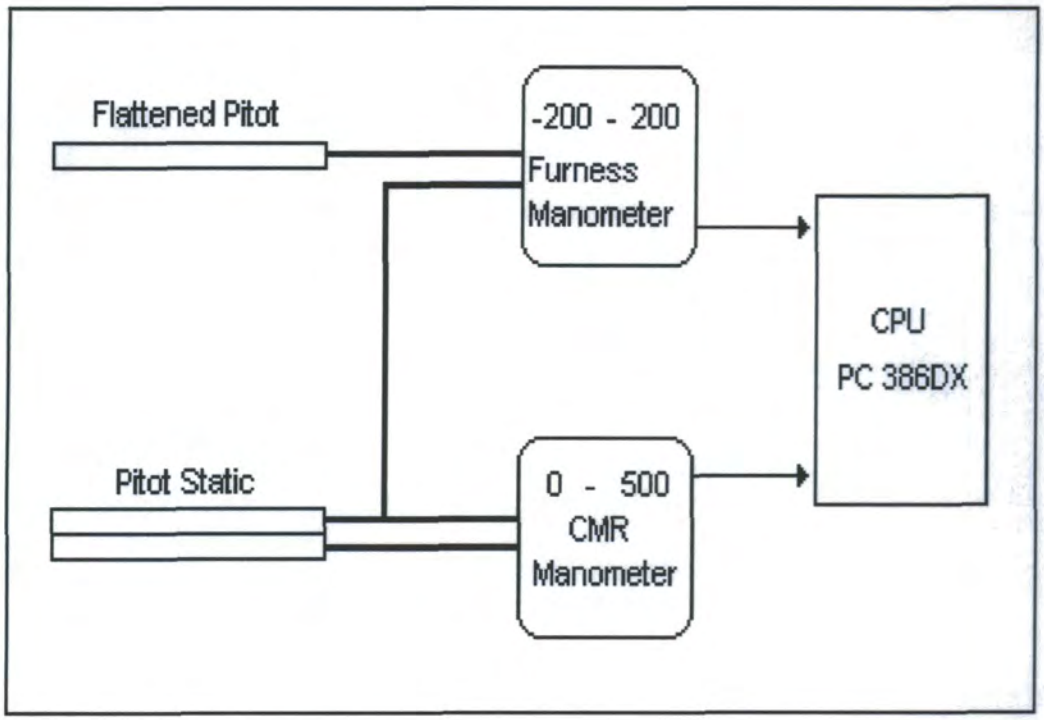

Figure 3.9: Flattened pitot probe transducer arrangement

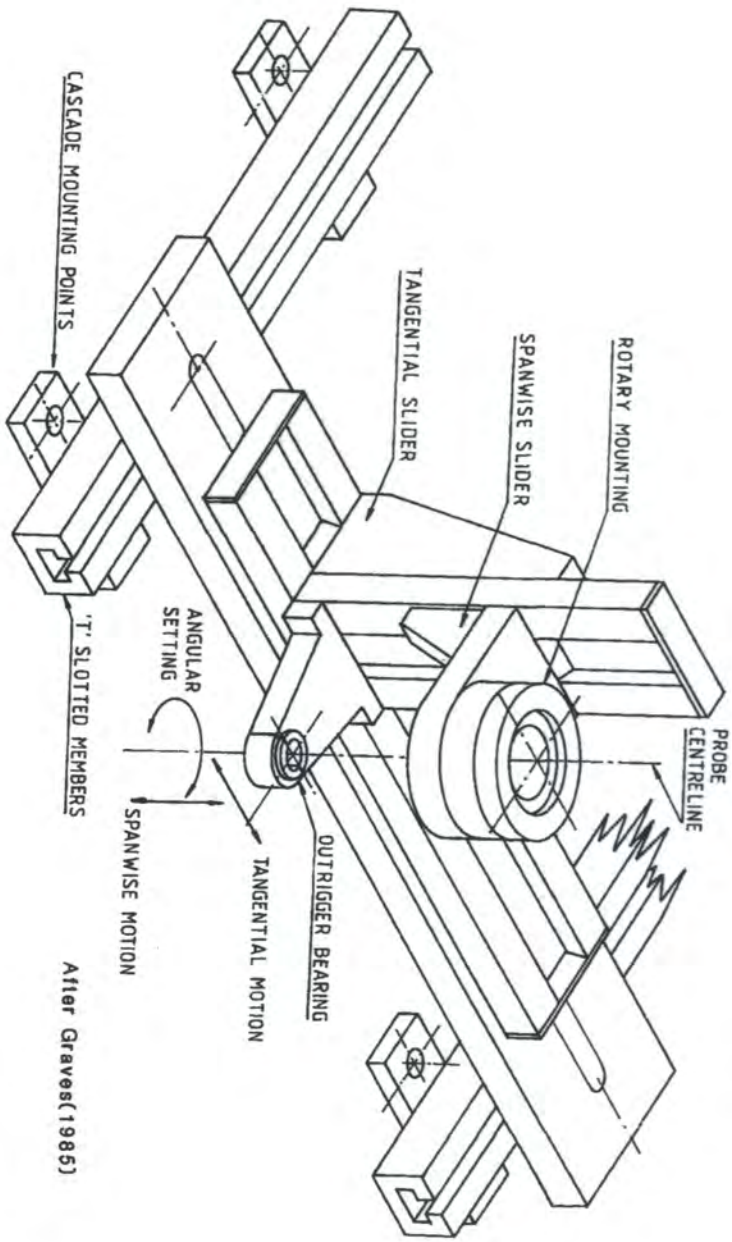

Figure 3.10: Traverse slides and rotary table

Chapter 4 : Experimental results

4.1 Introduction

This chapter aims to present the data collected from traverses made in the Alstom nozzle guide vanes cascade. Traverses were carried out in slot 09 using only the flattened pitot probe and in slot 10 for both planar and profiled end wall, using the five hole probe and the flattened pitot probe described in the apparatus chapter. The blades were fitted with a trip in order to achieve fully turbulent flow. The data collected from the two probes are processed and compared to results obtained by Yan [1999].

4.2 The mid span traverse

In order for the flattened pitot data to be used in addition to the five hole probe data for the mixed data calculations the two should at least agree at the point where the flattened pitot data are inserted in to the calculations and at mid span. As the results

agreed away from the end wall from 8mm to 10mm (see *Figure 4.20*) a mid span traverse was made with each of the probes to verify the agreement at mid span.

Yan's data and both the five hole and flattened pitot probe data are presented in *Figure 4.1*. The value for total pressure loss coefficient at mid pitch, mid span should approach zero. Yan shows higher losses at mid span as later shown in the pitch averaged graphs. The flattened pitot agrees on the level of loss with the five hole probe and at mid pitch mid span give an almost zero value for loss. The results from the flattened pitot probe are shifted to the right by approximately 20mm. This is maybe caused by a difference in the positioning of the tip of the flattened pitot probe, and experimental error in positioning the probe. The tip of the probe extends four millimeters from its center of rotation. Bearing this in mind when the probe is inclined by 77 degrees some of this shift can be justified. Therefore the two sets of data would coincide if this shift were to be dismissed.

4.3 Slot 09 Results

Slot 09 is the slot immediately downstream of the blades. This slot was traversed using the flattened pitot probe. Results obtained from these traverses are compared to results obtained by Yan [1999]. In *Figure 4.2* the total pressure loss area plots for the half span distance obtained by Yan [1999] can be seen. The two plots show the planar and profiled end wall total pressure loss. The accuracy of the measurements close to the end wall is not expected to be very high as the size of the five hole probe is such

that the blockage caused disturbs the flow close to the end wall. Furthermore the area that the end wall affects the most lies between 15 - 40mm from the end wall, where the profiled end wall gives a reduction in the loss peak. Similar reduction of loss could be expected for the area adjacent to the end wall although this would not be captured by the five hole probe.

4.3.1 Slot 09 planar end wall results

With the planar end wall fitted to the cascade the slot was traversed using the flattened pitot probe. The total pressure loss area plots are shown in *Figure 4.3*. Results from Yan [1999] clearly mark the two wakes the first peak being 75mm tangentially and the second approximately 210mm which agrees with the blade pitch which is 140mm. At 10mm from the end wall the loss coefficient has a value of 1.0 for the area between the two wakes whereas the area to the right of the second wake (at 210mm) this value reaches down to 2.5mm from the end wall. The peak of loss within the two wakes is between 3.0 and 3.5.

The second plot of *Figure 4.3* presents the data obtained with the flattened pitot probe. Similar to the first graph the two wakes are clearly marked. The center of the first wake, which is that of the bottom blade of the measured passage, is approximately at 65mm tangentially and the second wake also appears displaced by 10 -15mm to the left with its center approximately at 200mm. Although the placement

of the wake does not coincide with the wake position measured by Yan, the two wakes are approximately 135mm to 140mm apart

The flattened pitot total pressure loss at 10mm is lower than Yan by 0.5 although the loss follows same trend between and outside of the wakes. Close to the end wall the total pressure loss coefficient measured by the flattened pitot probe is 4.0, which is higher than that measured by Yan [1999]. Additionally judging by the increase in loss moving closer to the end wall the boundary layer thickness measured by Yan is not very clear, with an estimate of the boundary layer thickness of 6mm to 7mm. Using the flattened pitot the boundary layer is more clearly defined and the thickness measures between 4.5mm to 5.5mm.

Figure 4.4 shows the pitch averaged total pressure loss for both sets of data. The data by Yan were pitch averaged over the same area as the flattened pitot data, across a wake, whereas Yan originally calculated the pitch average coefficients by pitch averaging between the two wake peaks. Comparing the two, the flattened pitot data show a lower loss away from the end wall, whereas in the region of 0mm to 4mm the loss for the flattened pitot is higher from Yan's five hole probe measurements.

4.3.2 Slot 09 profiled end wall results

The cascade was fitted with the profiled end wall and close to the end wall traverses were made using the flattened pitot probe. These are compared to data by Yan [1999]. *Figure 4.5* showing the total pressure losses plots for both sets of data. The first plot (by Yan) shows the two wakes although the second is not clearly defined. The loss peak appears unchanged compared to the planar end wall results whereas a reduction in the boundary layer thickness is noted although not very clearly defined. The flattened pitot area plot presents more clearly defined wakes, however they appear to be shifted toward the left compared to Yan. The loss peaks within the wakes are of similar magnitude but differ in tangential extent, as the wakes measured with the flattened pitot are narrower.

The boundary layer thickness appears to be less than 1mm and the area between the two wakes shows a loss coefficient of 0.5 from 10mm radially down to the end wall. The peak of loss is reduced from 4 for the planar end wall down to 3.5 to 3 for the profiled. The pitch averaged results shown in *Figure 4.6* present a lower loss measured by the flattened pitot compared to the overestimated loss by Yan although the peak is approximately the same adjacent to the end wall.

Comparing the planar and profiled end wall pitch averaged results the flattened pitot predicts a much higher reduction in loss close to the end wall which is not present in Yan's data. *Figure 4.7* is showing the half span data along with a larger scale view of the 0-60mm area.

4.4 Slot 10 planar end wall

The slot was traversed over the half span distance using the five hole probe. Additionally close to the end wall traverses were made with the flattened pitot probe, producing two sets of data.

Area plots were produced for both data sets. The total pressure loss area plot and the yaw angle variation over the half span are presented in *Figure 4.8*. The two wakes from the main passage can clearly be seen, although the first wake, caused by the bottom blade of the measured passage on the left hand side of the graph, was not totally captured by the traverse.

The total pressure loss area plot suggests that the two wakes differ in size. The wake from the second blade appears to cover a wider area, although the total pressure loss coefficient in the two wakes is of the same magnitude. Between the two wakes there is no variation of the loss, which compared to the wake loss is smaller by several orders of magnitude. At half span (200mm) and down to 60mm from the end wall there is no variation of the loss within the wakes as well as across the pitch. A loss core is observed in the area close to the end wall (0mm to 50mm) within each wake. Concentrating on the wake of the top blade, which is fully captured by the five hole probe, the peak of the loss core can be seen at 40mm in the radial direction and 225mm tangentially. Closer to the end wall the area within 10mm to 15mm away from the end wall shows a high loss due to the end wall boundary layer.

The yaw angle contour plots show the variation of the exit angle from the blade row. At mid span the angle is approximately 77 degrees. Some overturning is observed within the wakes with little or no variation in between.

The area up to 60mm from the end wall shows a wider yaw angle variation. Five degrees of underturning can be noted at the peak approximately 30mm from the end wall. Closer to the end wall the exit yaw angle reaches -82 degrees producing 6 degrees of overturning at its peak. The two areas of overturning and underturning coincide with the area were the peaks total pressure loss are observed.

The same flow phenomena can be seen more clearly in *Figure 4.9* showing the area within 50mm from the end wall where the widest yaw angle and loss variation is observed. The loss core of the main wake lies between two areas of underturning. As the underturning gradually reduces moving towards the end wall the start of the overturning coincides with the rise in total pressure loss due to the boundary layer. The boundary layer as captured by the five hole probe has its edge 10mm from the end wall.

Data by Yan [1999] are presented in *Figure 4.10*. The wakes from the main blade passage are present and as with the five hole probe data (*Figure 4.8*) the wake from the top blade is not fully captured. The amount which the two wakes extend across the pitch and their position matches the five hole probe data presented in *Figure 4.8*. Comparing the fully captured wake of *Figure 4.8* to that of *Figure 4.10* the most

noticeable difference is the higher loss at mid span within the wake measured by Yan. (Also seen in *Figure 4.1*). However the peak of the loss core captured by the five hole probe is higher by 0.5 than that measured by Yan, whereas the two coincide in terms of their position.

The loss between the two wakes away from the end wall is of similar magnitude but in the region within 50mm from the end wall the loss measured by Yan is higher than that of the five hole probe. At mid pitch the total pressure loss coefficient for the five hole probe reduces down to 0.5 at 20 mm from the end wall were Yan shows a total pressure loss coefficient twice as big. The mid span traverse shown in *Figure 4.1* shows this difference as well.

The yaw angle contours from both sets of data present identical flow patterns although the overall level of angle suggests that the five hole probe data show a lower exit angle and regions of higher underturning and overturning than that of Yan.

Closer to the end wall, *Figure 4.11,* by Yan suggests that the boundary layer has the same thickness as that measured by the five hole probe. Furthermore the overturning observed within the boundary layer is initiated in the same region for both figures. The areas of overturning and underturning for *Figure 4.9* and *Figure 4.11* appear very similar for both sets of data.

The area close to the end wall (up to 10mm) was traversed with the flattened pitot probe for a more detailed view of the total pressure loss within that area. The data collected are presented in *Figure 4.12* for comparison with the five hole probe total pressure loss over the same area. Due to the bigger size of the five hole probe measurements were only taken from 3mm outwards. The loss peak obtained by the five hole probe is higher by 0.5 to that of the flattened pitot traverse, where a small shift in the position of the peak of the wake loss is observed. The peak is displaced by 20mm to the right but the overall image suggests that the same flow phenomena are picked up as the contours for both the plots follow the same trends.

Data from the two probes were pitch averaged over the 140mm pitch. The pitch averaged total pressure loss for the planar end wall is presented in *Figure 4.13* for comparison to the pitch averaged data from Yan. The total pressure loss from the five hole probe and the flattened pitot is lower than the loss presented by Yan. Whereas Yan shows the same position for the peak in loss at 30mm radially and the same trend being followed towards the end wall, the level of loss is different. The flattened pitot data agree well with the five hole probe data. The loss reduces more steeply moving away from the end wall than Yan's data reaching at a minimum value close to that at mid span, whereas Yan's data do not reduce to that value.

The pitch averaged yaw angle shows a higher exit angle by Yan at mid span by approximately 0.5 to 0.8 of a degree. The areas of overturning coincide for both Yan and the five-hole probe data whereas the latter show a higher peak of underturning and a small displacement of 5mm towards mid-span. The two sets of data agree that

the yaw angle reaches a constant value at 50mm to 60mm and retains that value until mid span.

Mixed data area averaged values are derived by using data from the flattened pitot probe for the area between 0mm and 10mm and adding to these data the five hole probe data from 10mm to 200mm. By this method a more accurate view of the overall loss is achieved by adding the loss close to the end wall. The area averaged values presented in *Table 4.1*, along with the inlet loss as measured by Yan, support the finding of *Figure 4.13* as the loss by Yan is higher than both the five hole probe and the mixed data area averaged values. However due to a higher mid span loss by Yan the secondary loss appears less than that for the five hole probe and the mixed data. The mixed data give the highest secondary loss as expected due to a higher area of loss measured by the flattened pitot probe.

4.5 Slot 10 profiled end wall

With the profiled end wall fitted to the cascade, slot 10 was traversed with the probes used for the planar end wall traverses. Additionally mid span traverses where made using the two probes in order to verify the agreement of the two probes at mid span as seen in *Figure 4.1*

The area plots obtained from the five hole probe traverse are presented in *Figure 4.14.* The total pressure loss contours show the two wakes from the main passage

measured. The loss in the two wakes has the same magnitude although the wake from the top blade shows some areas of higher loss. The second wake covers a wider area than the bottom blade wake, although the loss is less within the wake. The profiled end wall should not have any significant effect to the loss at mid span. Comparing the planar end wall data of *Figure 4.8* to the profiled end wall data of *Figure 4.14* there is very good agreement in the position of the wakes as well as the level of loss. From half span to 60mm from the end wall there is little variation of the total pressure loss.

Between the two wakes the loss variation is minimal reaching a constant value from mid span, carrying the same value across the span up to 20mm from the end wall. The loss core appears 60mm from the end wall with a peak of 2.5 30mm away from the end wall.

The half span yaw angle contours of *Figure 4.14* show a mid span value of -74 to -75 degrees. In comparison to the planar end wall data of *Figure 4.8* there is less variation of angle at mid span and the overall level is lower by 1 to 2 degrees. This is believed to have resulted by the manual measurement of the yaw angle and the level of error associated. However the variation of yaw angle in *Figure 4.14* coincides with the areas of total pressure loss variation. The yaw angle does not vary across the span from 200mm down to 50mm. The flow appears to underturn for a region between the two wakes in the area within 50mm from the end wall. This is gradually turned to overturning moving closer to the end wall. The peak of underturning is of 2 to 3 degrees and the same amount of overturning is observed adjacent to the end wall.

The area of high total pressure loss, and yaw angle variation, is presented in *Figure 4.15*. The total pressure loss area plot suggests that the boundary layer thickness is between 10mm and 12mm and the peak loss coefficient close to the end wall is 2.5. The yaw angle plot shows a peak of underturning of -70 for a small area at the base of the main wake and a peak of overturning of -80 degrees. The flow angle within the boundary layer is always higher than that of the mid span flow.

Comparing *Figures 4.14 and 4.15* to data by Yan presented in *Figures 4.16 and 4.17*, the five hole probe traverse gives a generally lower total pressure loss than Yan although for a large area between the two wakes the two give the same value for loss. Yan shows a thicker boundary layer by 2mm to 3mm and a higher total pressure loss coefficient by 1.0 in the peak of the loss core. The yaw angle variation is much less for Yan as well as the overturning. The underturning is between 2 to 3 degrees which is very similar to the five hole probe data.

The five hole probe data *(Figure 4.14, Figure 4.15)* give lower values of loss compared to Yan *(Figure 4.1, Figure 4.17)*. When compared to the planar end wall results *(Figure 4.8, Figure 4.9)* of the same probe some significant differences can be seen which are believed to be the effect of the profiled end wall. Between mid span and about 70mm from the end wall the two sets of are almost identical in terms of total pressure loss. The region that the profiled end wall has affected the most is the area within 60mm from the end wall. The loss core peak has been noticeably reduced by one third of its planar end wall value. Although no change can be identified in the boundary layer thickness the total pressure loss contours show a reduction of the loss

moving toward the end wall. There the reduction is more obvious reaching almost one third of the peak loss.

The yaw angle variation contours clearly mark the effect of the profiled end wall showing less variation of the angles pitchwise and a relatively small reduction in the overturning and underturning.

The flattened pitot total pressure area plot presented in *Figure 4.18* against the five hole probe data shows a big difference between the two in the boundary layer thickness. The flattened pitot shows more clearly defined wakes as well as the higher loss peaks, which is similar to the effect of the end wall as seen in slot 09 (*Figure 4.5*) Comparing the planar end wall results to the profiled for the flattened pitot *(Figure 4.12, Figure 4.18)* the boundary layer thickness is reduced from 10mm to 2.5mm and the area between the wakes reveals a much lower loss which should affect both the pitch averaged and the area averaged values.

The pitch averaged data presented in *Figure 4.19* show a big difference between Yan and the new five hole probe data and the flattened pitot data, as suggested by the area plots. Although both the flattened pitot data and the five hole probe present a higher peak of loss close to the end wall than Yan, the flattened pitot total pressure loss reduces very steeply in the first 3mm and then retains a much lower value until 8mm to 10mm where it matches the value from the five hole probe.

The pitch averaged yaw angle reveals a level difference between Yan and the new five hole probe data of approximately 0.9 of a degree. The most noticeable difference though is that the five hole probe data show a wider peak of underturning between 15mm and 25mm radially, where as the extent of overturning is lower for Yan.

The pitch averaged total pressure loss for both planar and profiled end wall is presented in *Figure 4.20*. The effect of the profiled end wall is noticeable in the areas between 0mm to 60mm (lower graph) where the profiled end wall gives a much lower loss peak. Furthermore the difference between the flattened pitot data is even bigger than for the five hole probe. *Figure 4.21* presents the pitch averaged yaw angle both end walls where a 0.8 degrees difference is noted at mid span which is carried until 60mm from the end wall. The peak of underturning is moved closer to the end wall and the overturning is reduced by 2 degrees.

The area averaged data shown in *Table 2* show the differences present in the pitch averaged results between Yan and the five hole probe data and the effect of using mixed data for a more accurate view of the loss in the area close to the end wall.
In the same table the reduction in secondary losses made by using the profiled wall is presented for all three sets of data. The mixed data show a bigger reduction both from Yan and from the five hole probe data alone.

Planar end wall				
Data	Area average Cpo	Mid span loss	Gross secondary loss	Net secondary loss
Yan 5 hole	1.0400	0.8884	0.1516	0.1306
5 hole	0.7232	0.5516	0.1716	0.1506
Mixed Data	0.7459	0.5516	0.1943	0.1733
Inlet loss	0.0210			

Table 4.1: Area averaged results for planar end wall slot 10

Yan 5 hole	0.9967	0.8800	0.1167	0.0957
5 hole	0.6626	0.5749	0.0877	0.0667
Mixed Data	0.6684	0.5749	0.0935	0.0725
Gain from profiled end wall				
Data	Net secondary loss reduction		Reduction (% of planar)	
Yan 5 hole	0.0349		23%	
5 hole	0.0839		49%	
Mixed Data	0.1008		52%	

Table 4.2: Area averaged results for profiled end wall slot 10

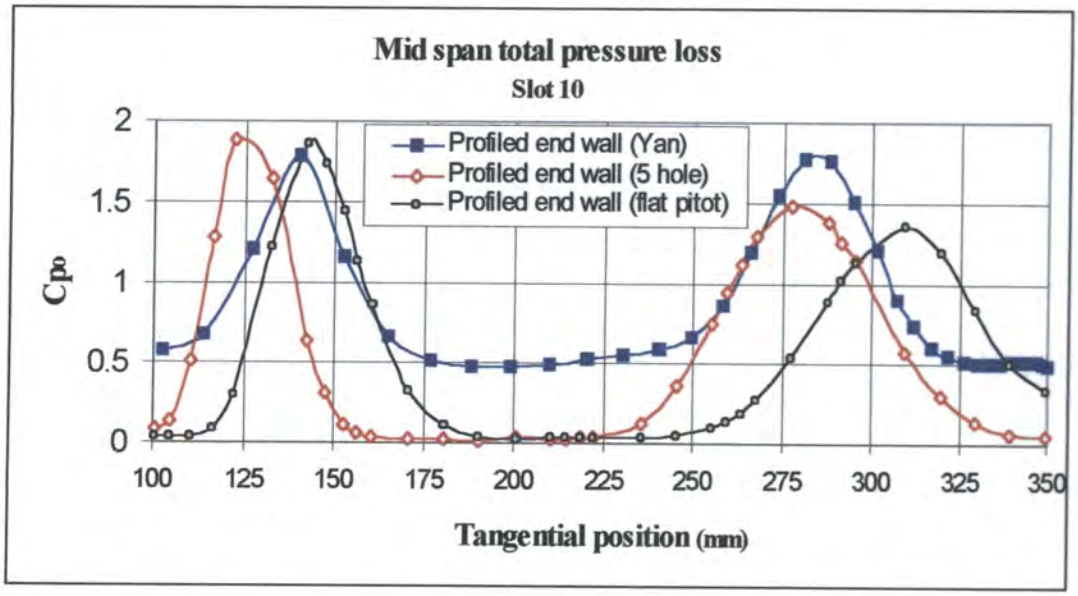

Figure 4.1: Mid span total pressure loss

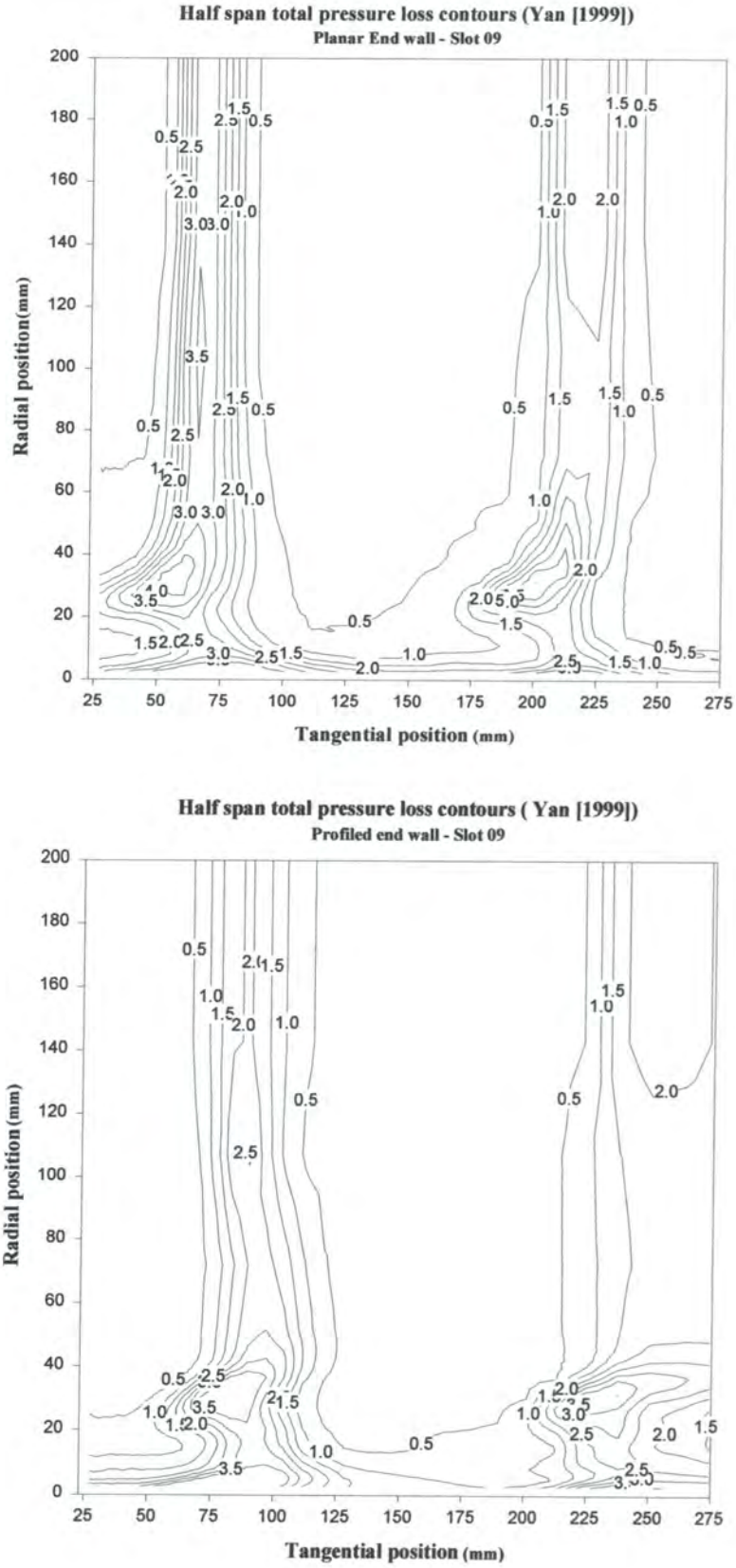

Figure 4.2: Half-span total pressure loss area plots (Yan [1999])

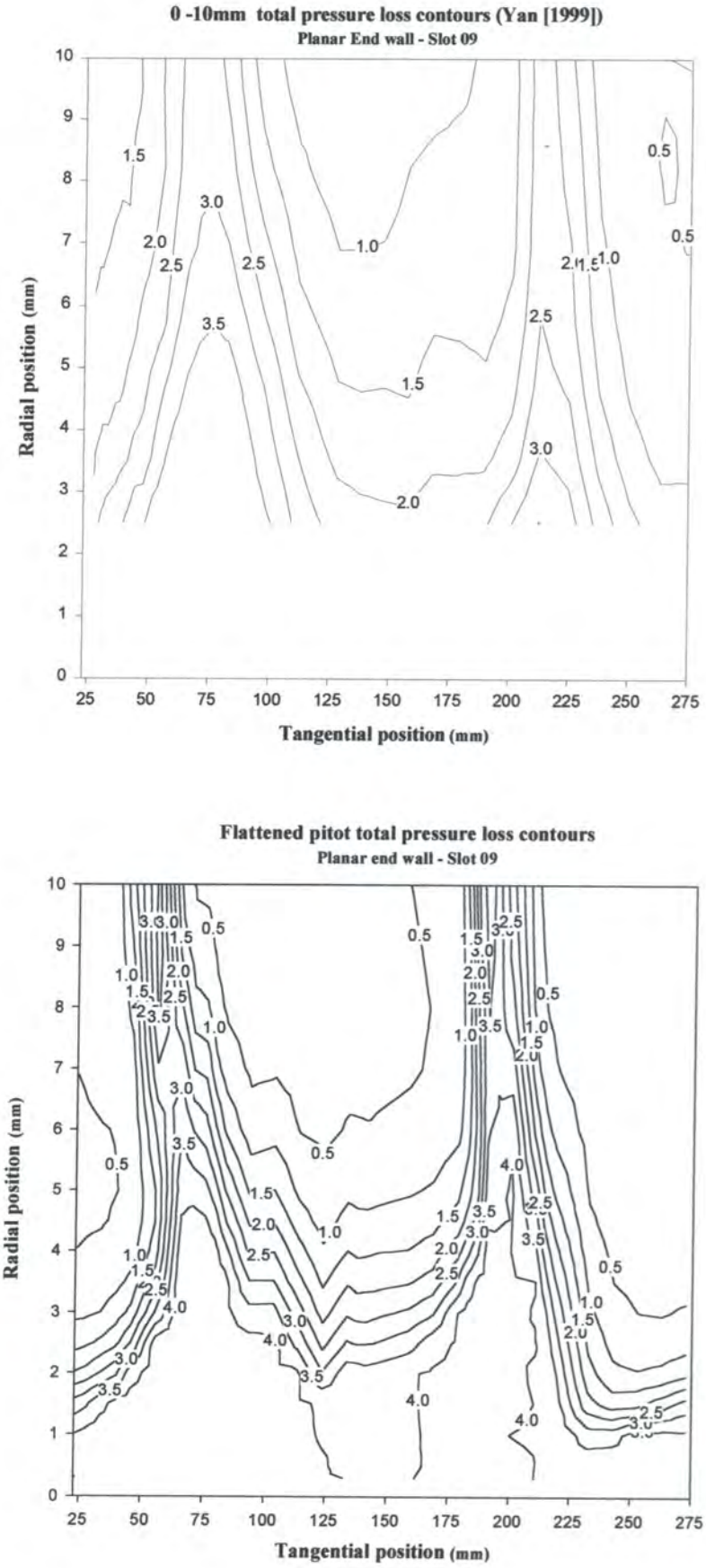

Figure 4.3: 0-10mm total pressure loss area plots

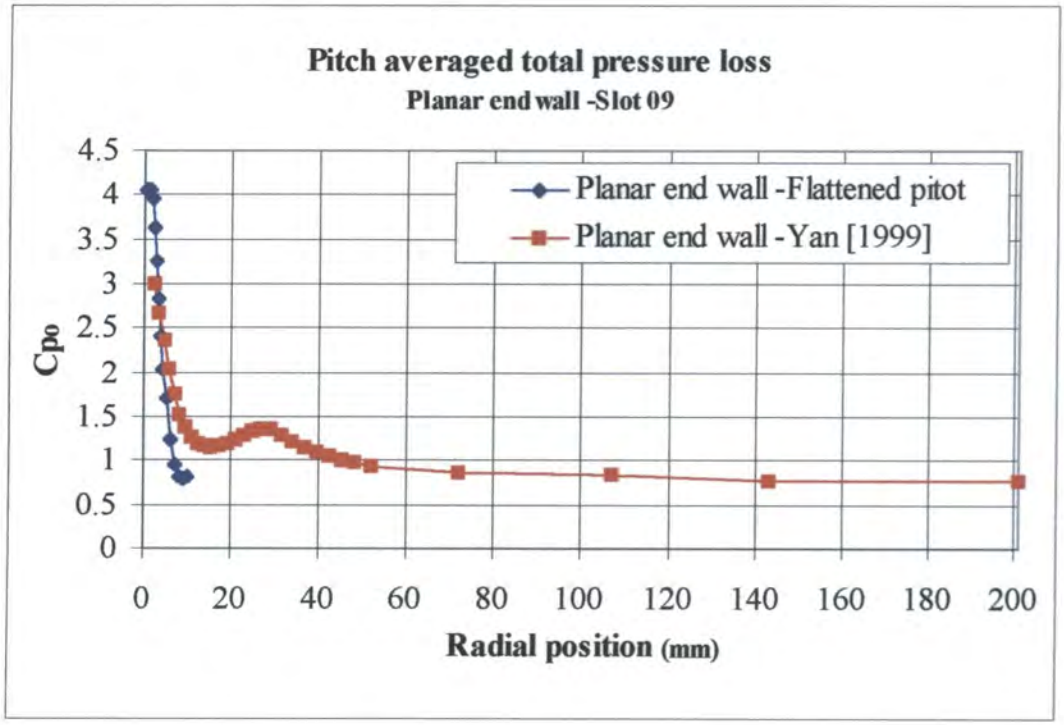

Figure 4.4: Planar end wall pitch averaged slot 09

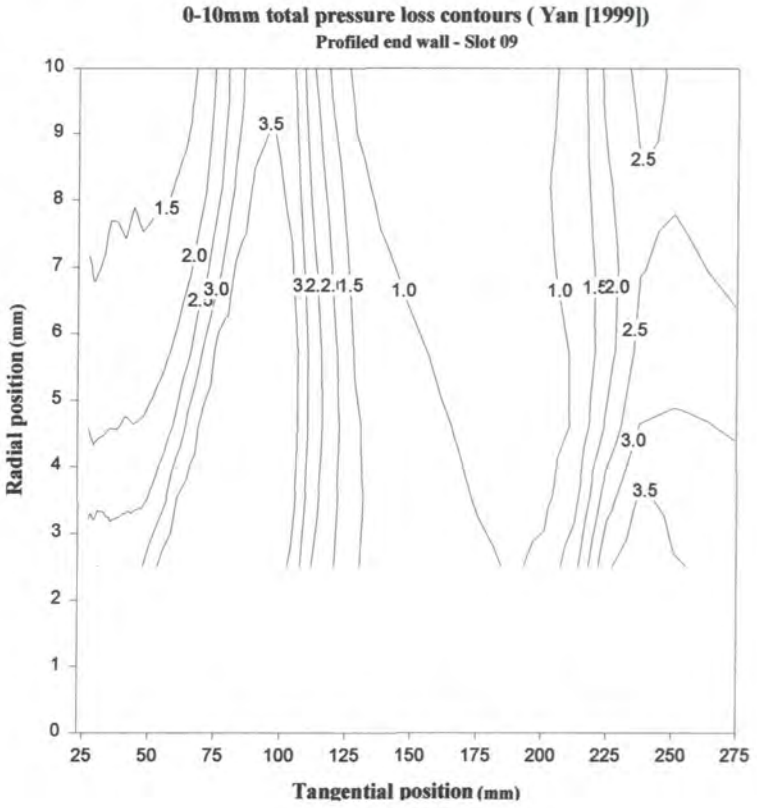

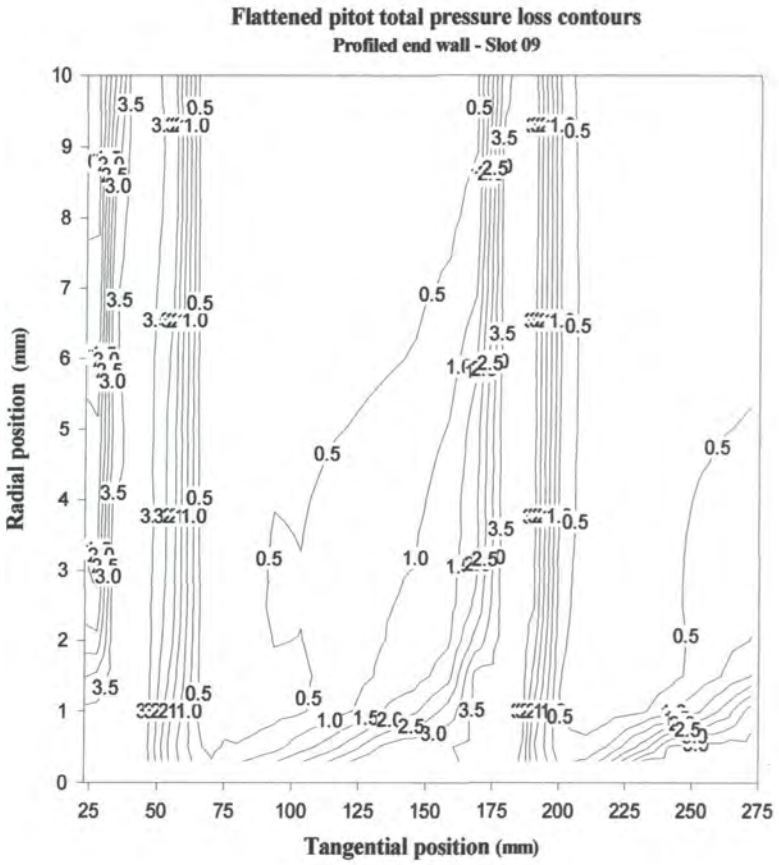

Figure 4.5: 0-10mm total pressure loss area plots

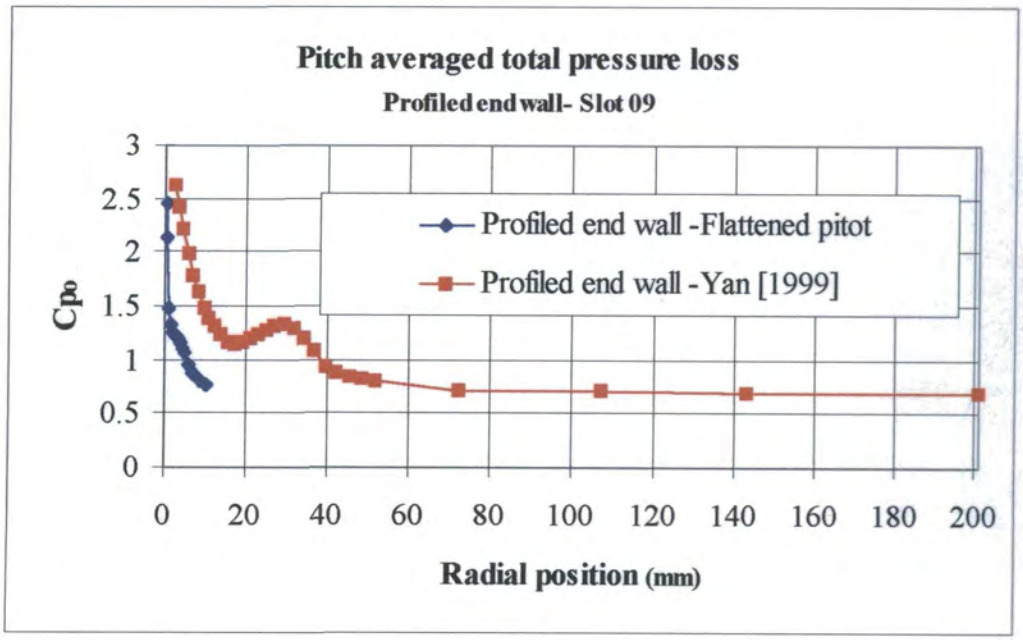

Figure 4.6 Profiled end wall pitch averaged slot 09

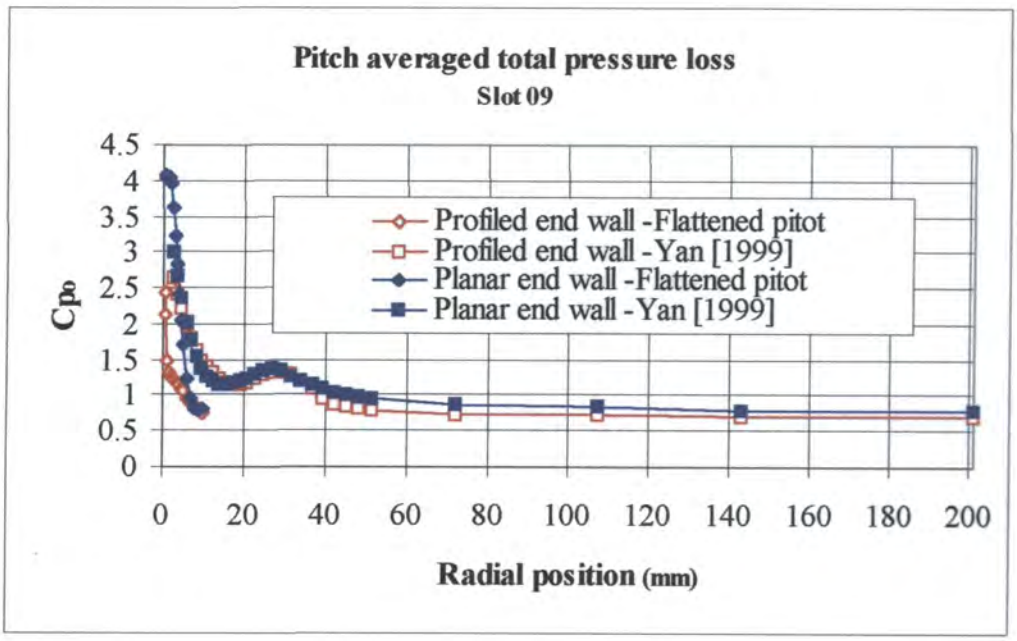

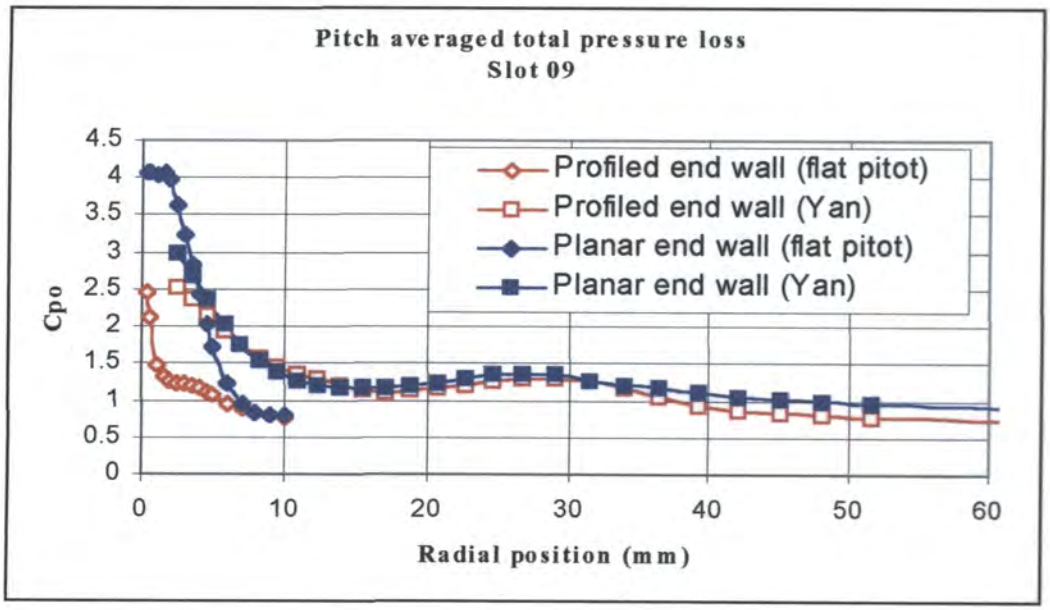

Figure 4.7: Pitch averaged results slot 09

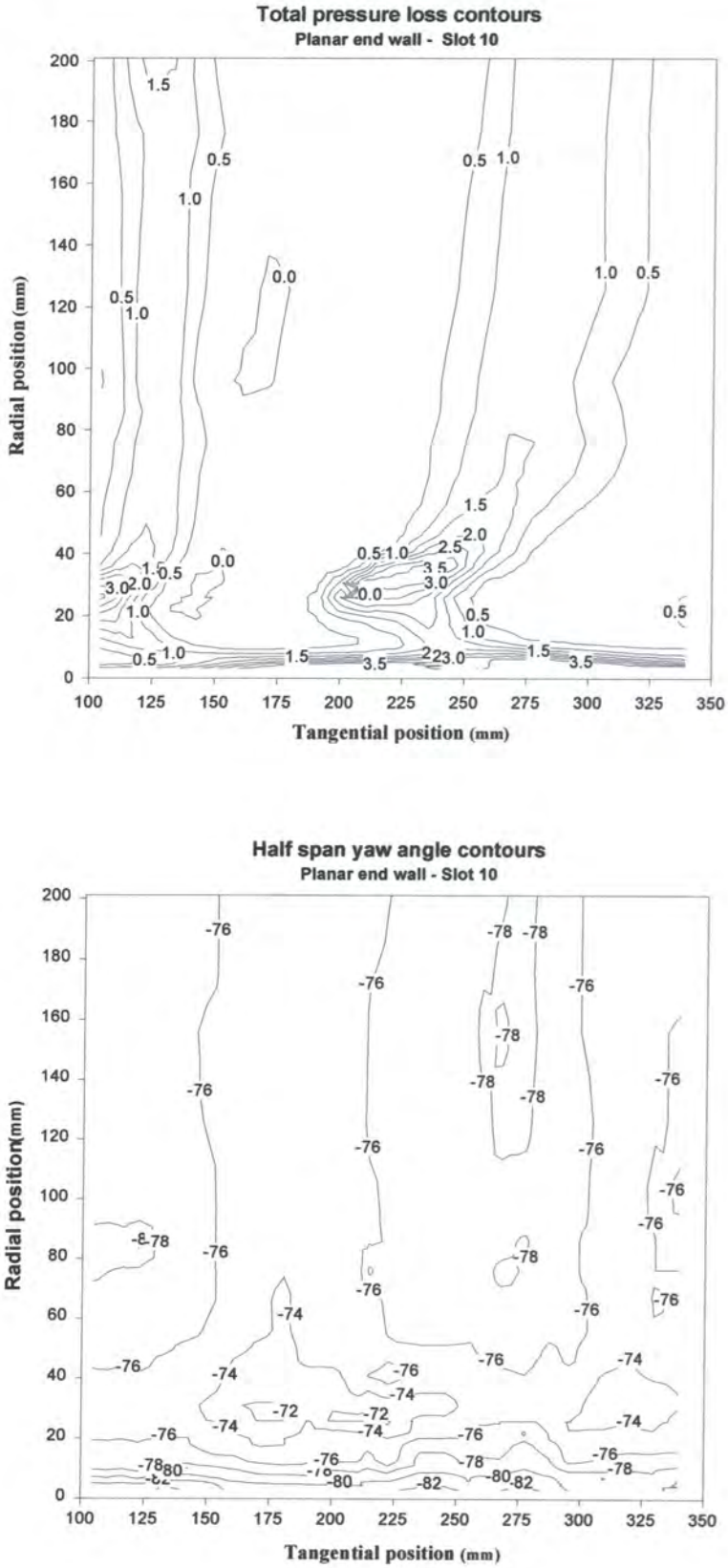

Figure 4.8: Planar end wall area plots

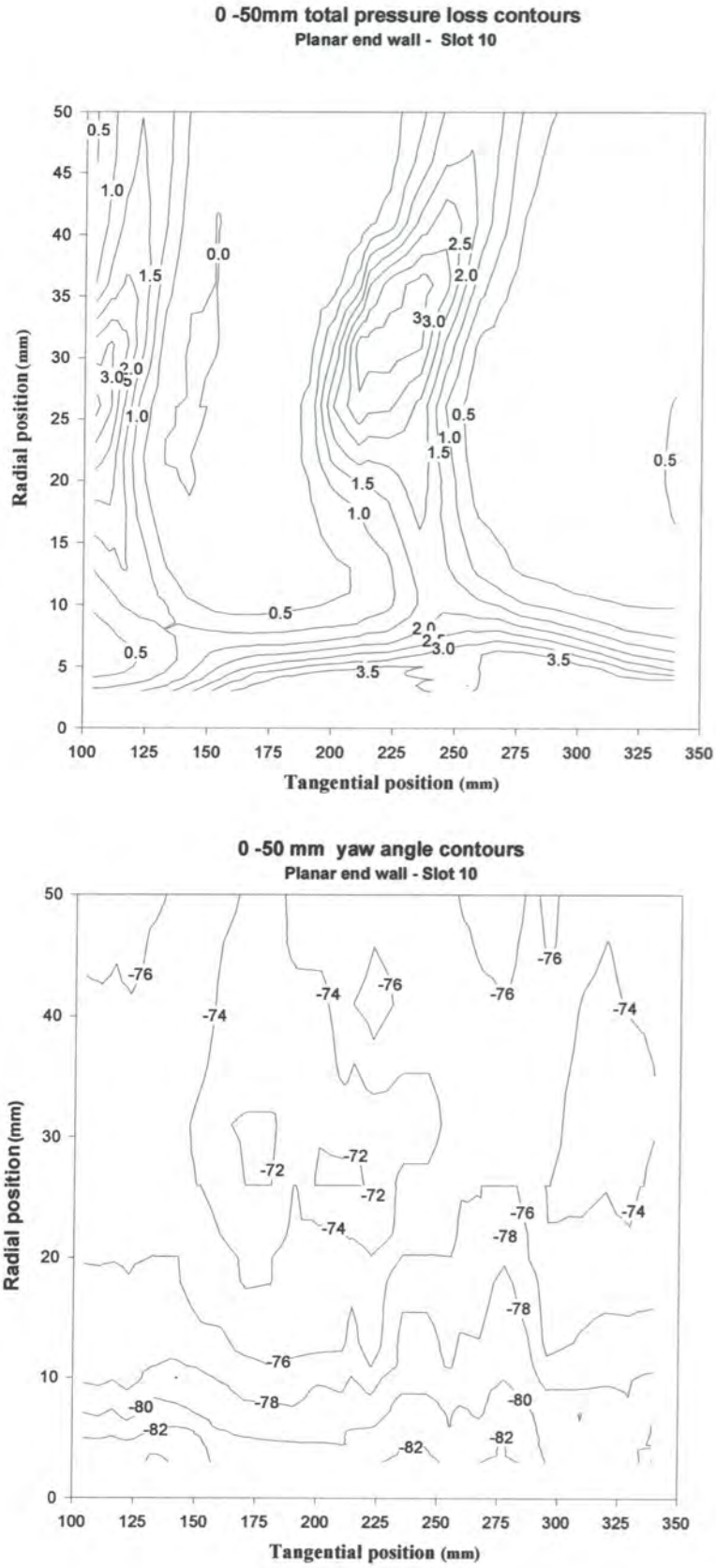

Figure 4.9:Planar end wall 0 –50mm area plots

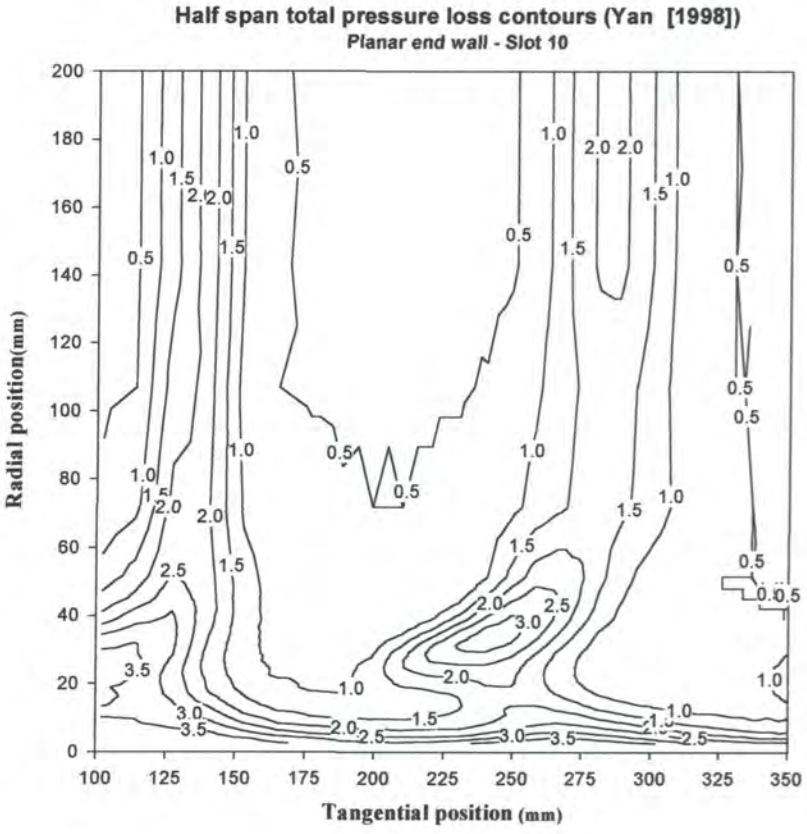

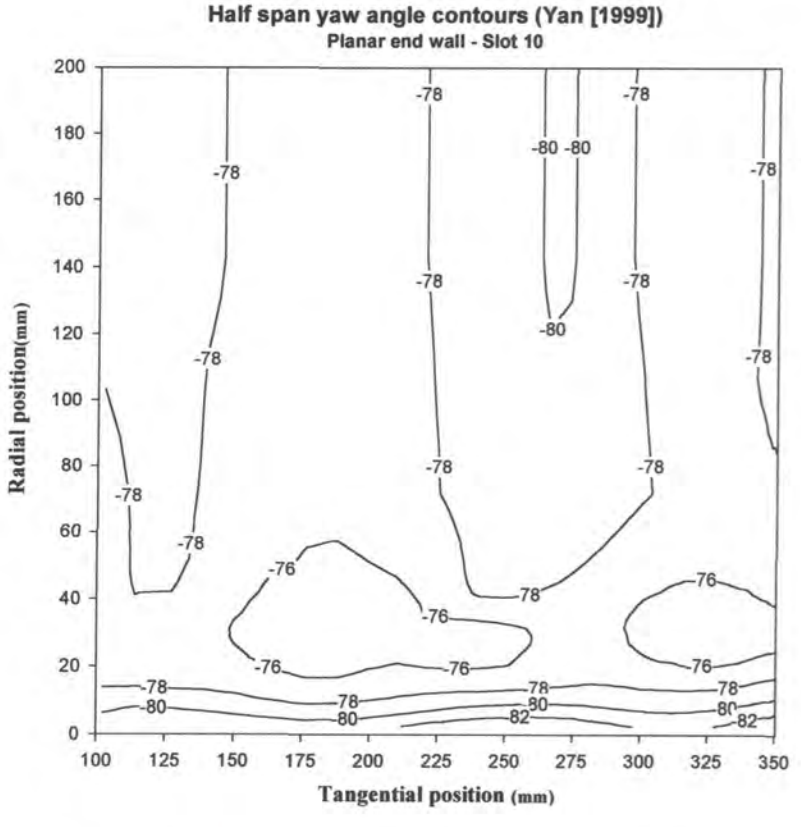

Figure 4.10: Planar end wall area plots (Yan 1999)

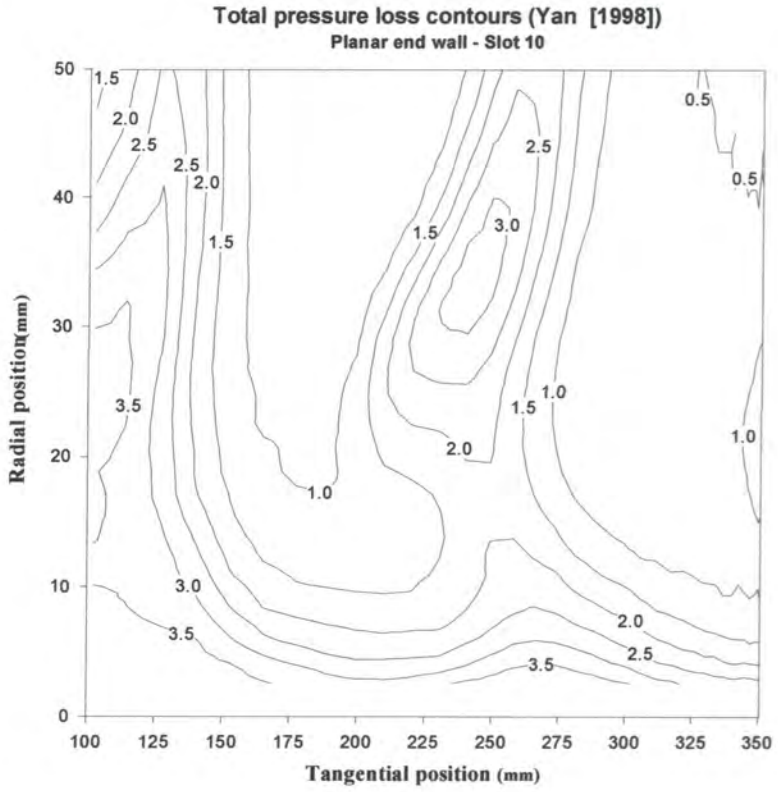

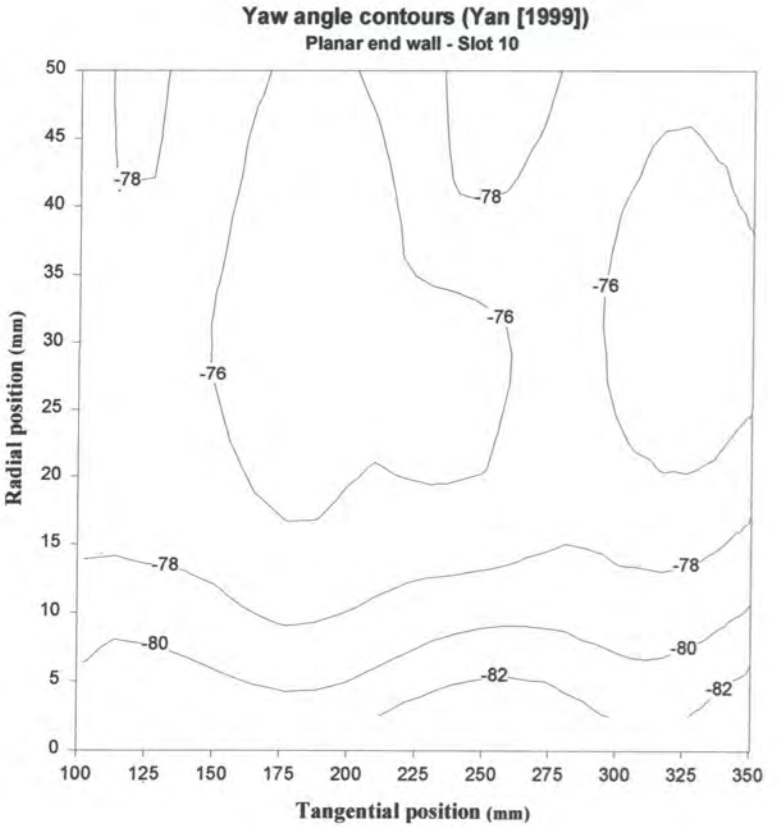

Figure 4.11: Planar end wall 0-50mm area plots (Yan 1999)

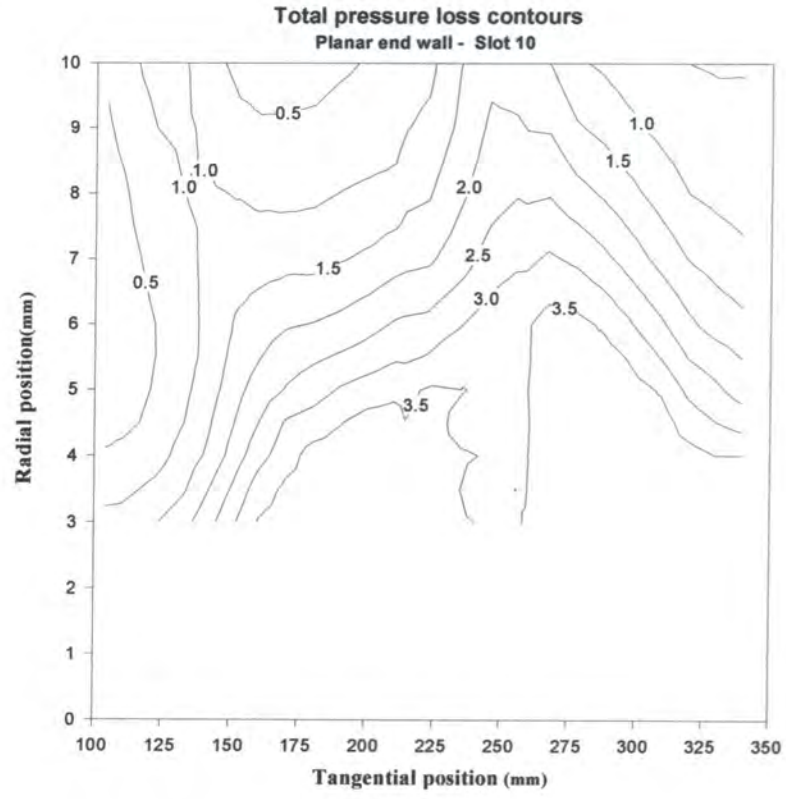

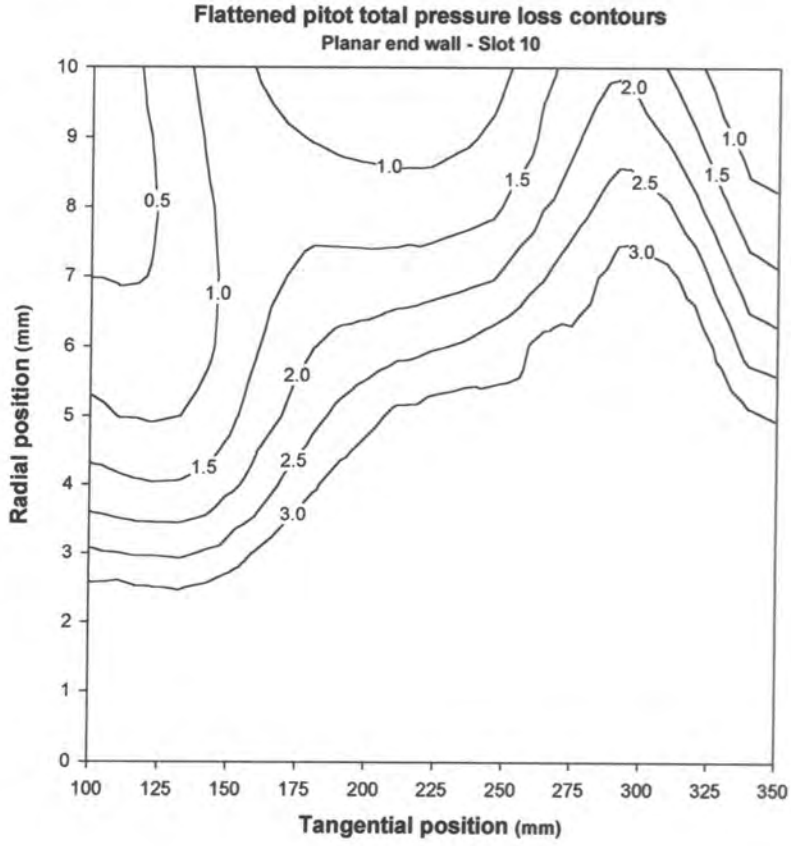

Figure 4.12: Planar end wall 0-10mm area plots

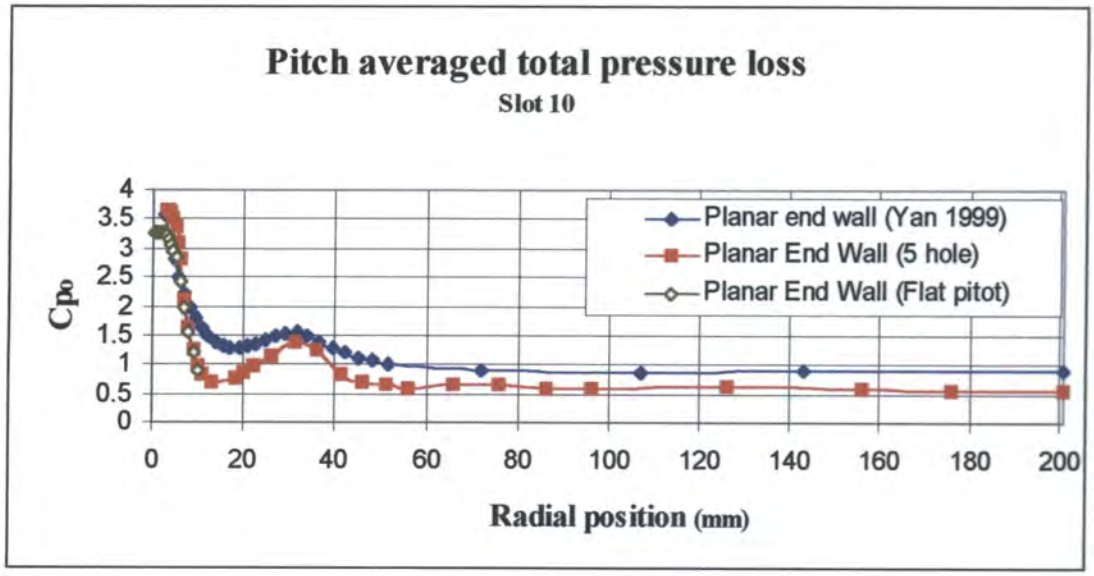

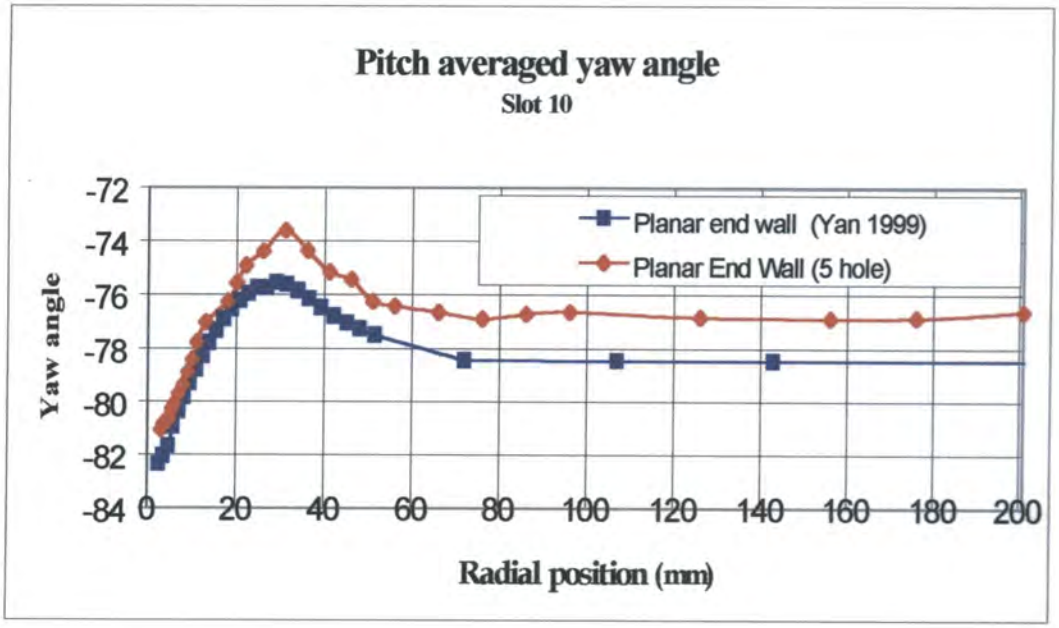

Figure 4.13: Planar end wall pitch averaged data

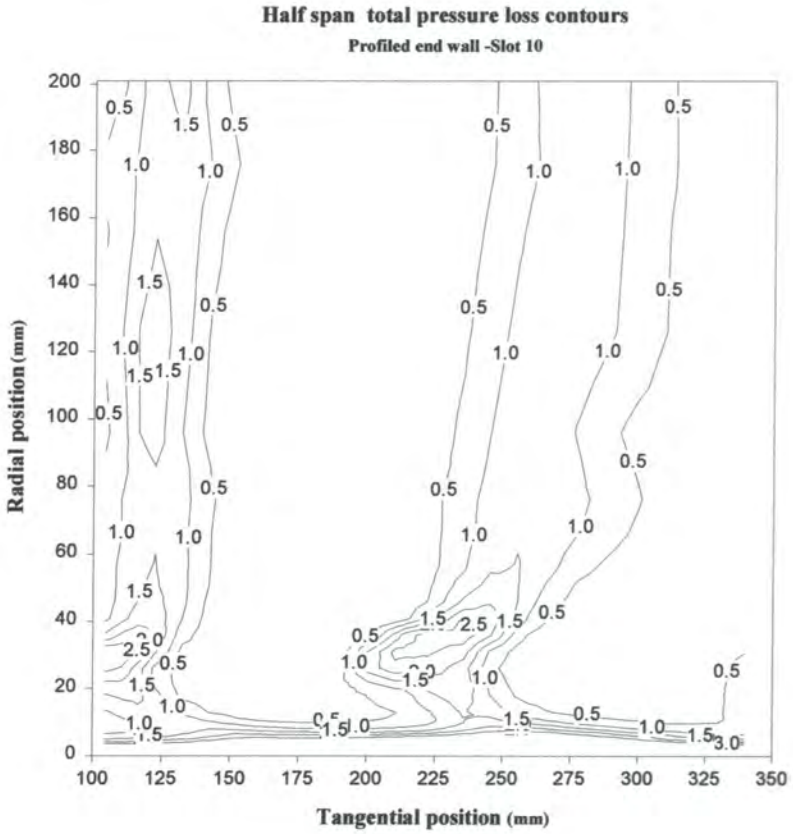

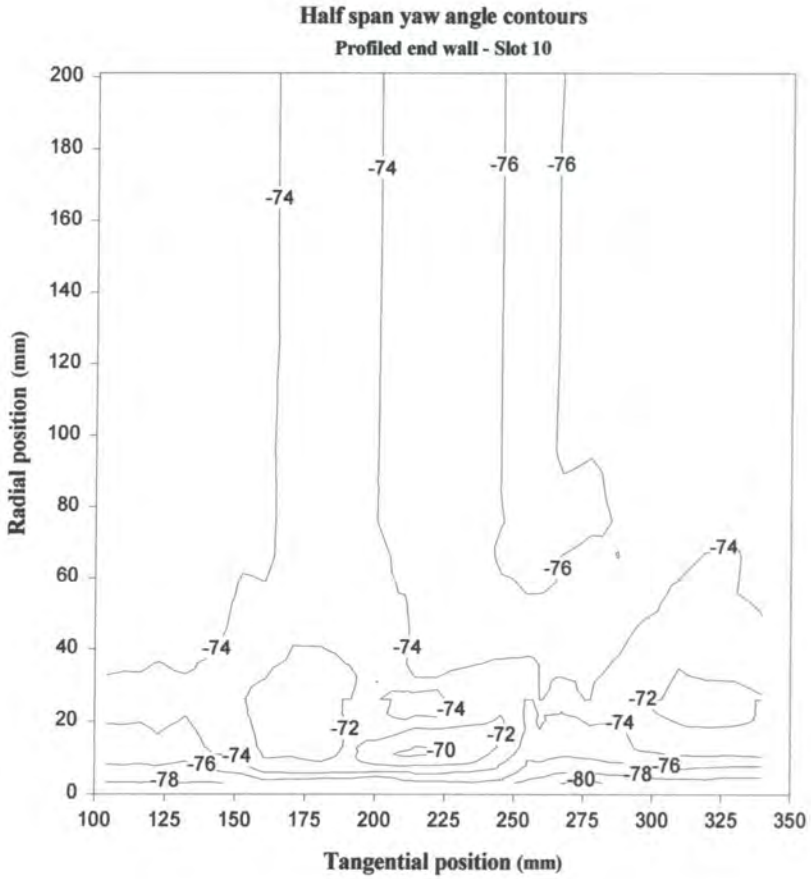

Figure 4.14: Profiled end wall half span area plots

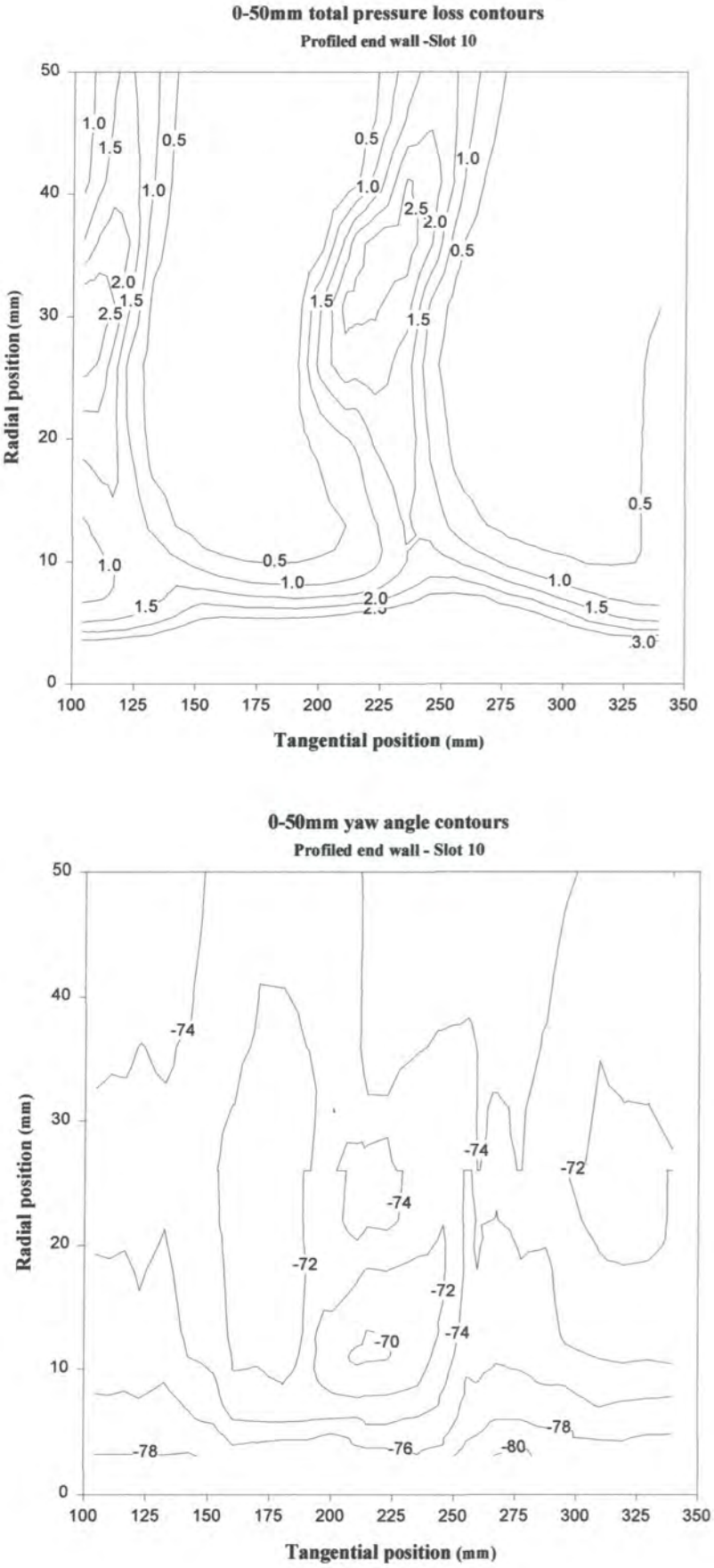

Figure 4.15: Profiled end wall 0 –50mm area plots

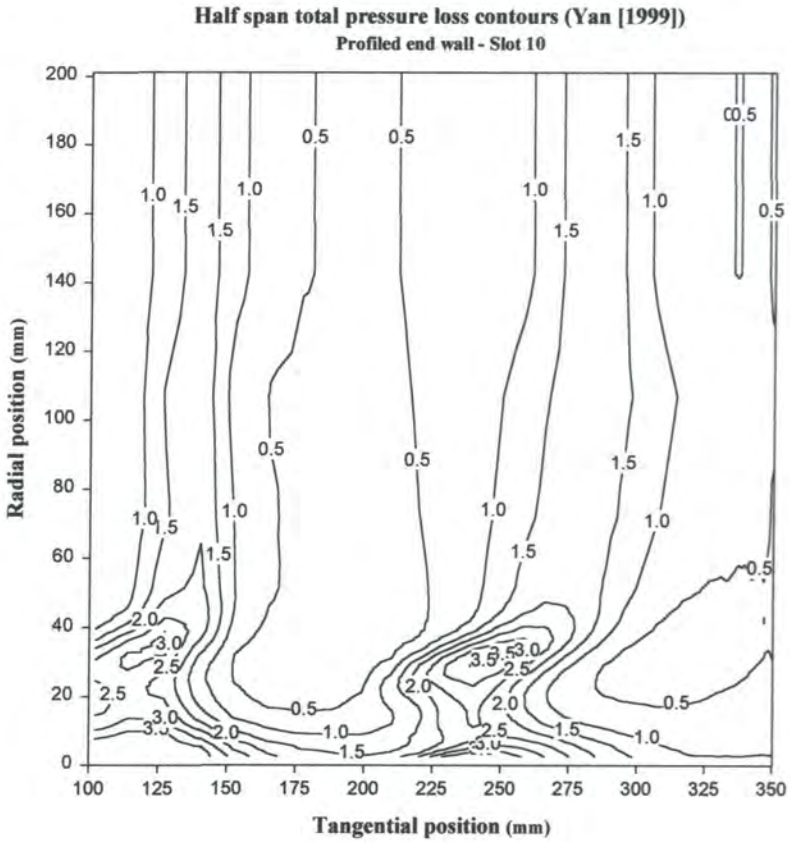

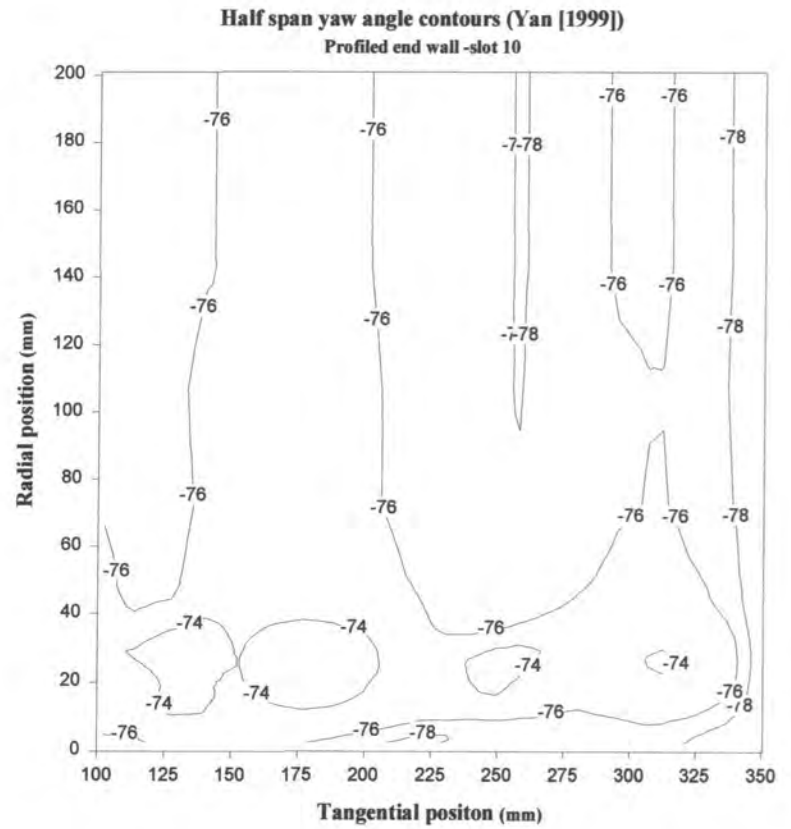

Figure 4.16: Profiled end wall half span area plots (Yan [1999])

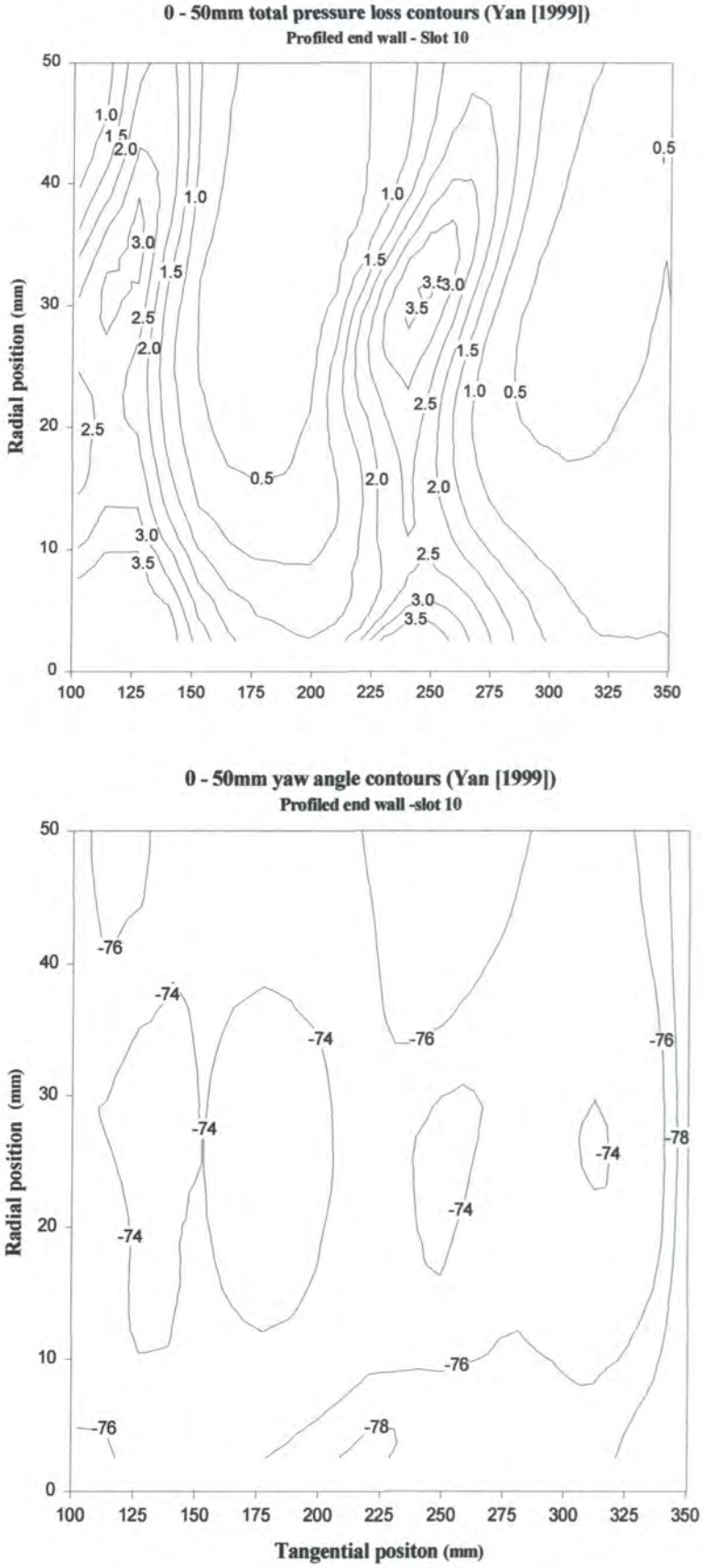

Figure 4.17: Profiled end wall 0- 50mm area plots (Yan [1999])

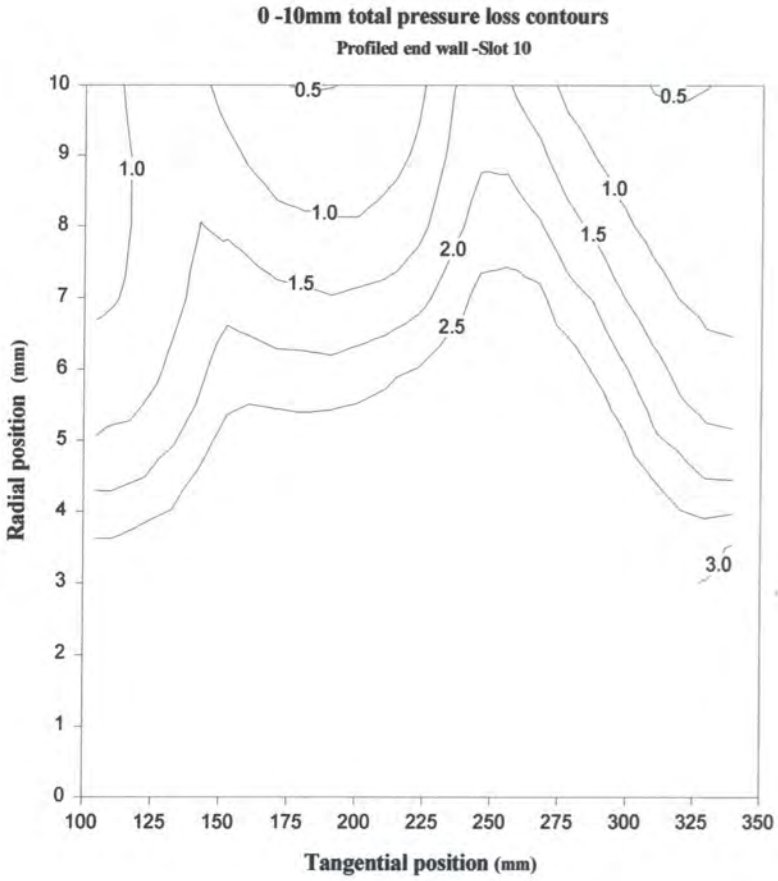

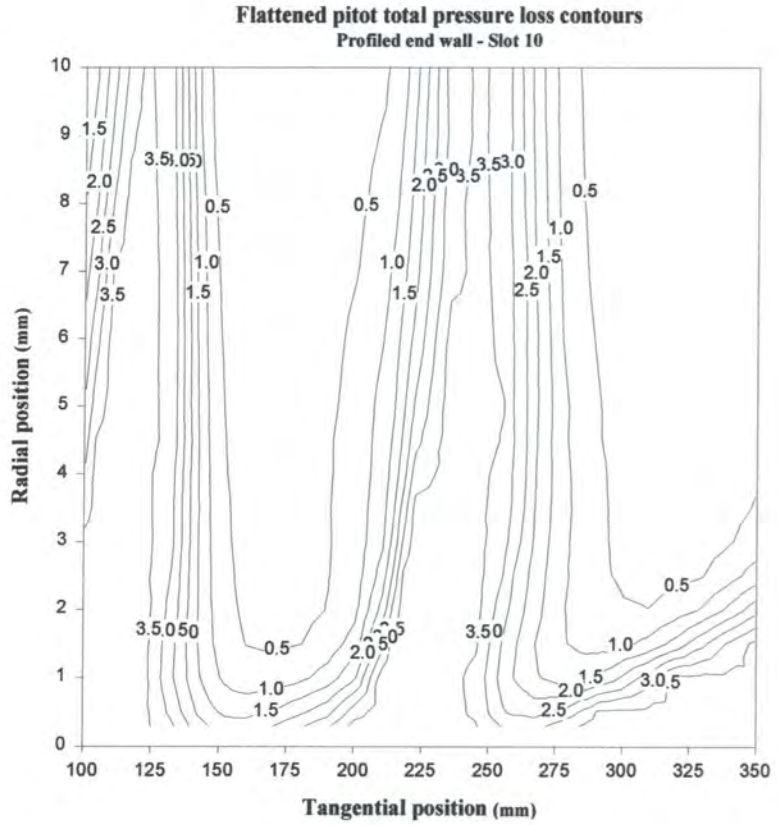

Figure 4.18: Profiled end wall 0-10mm area plots

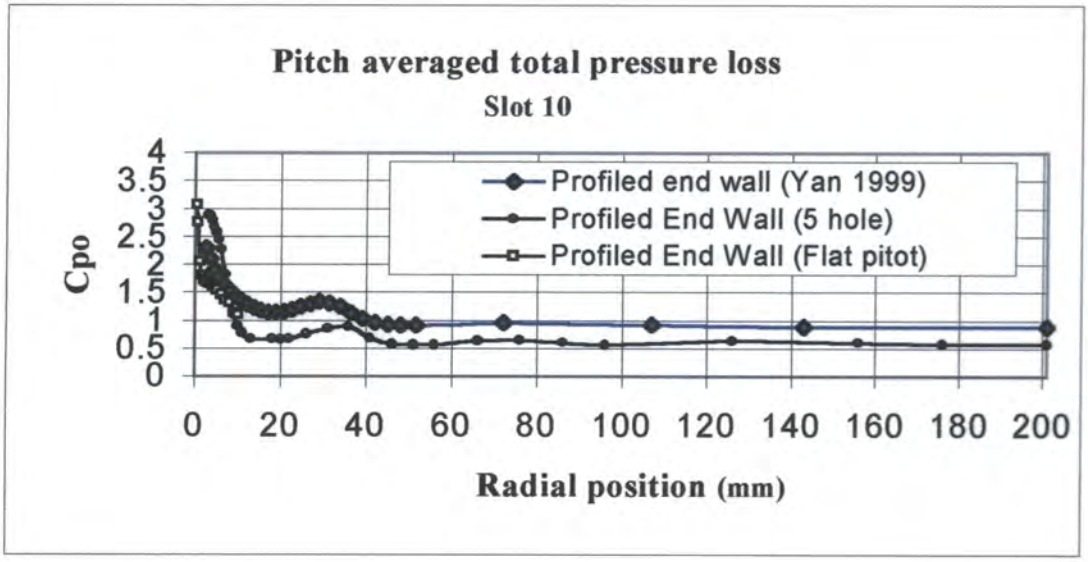

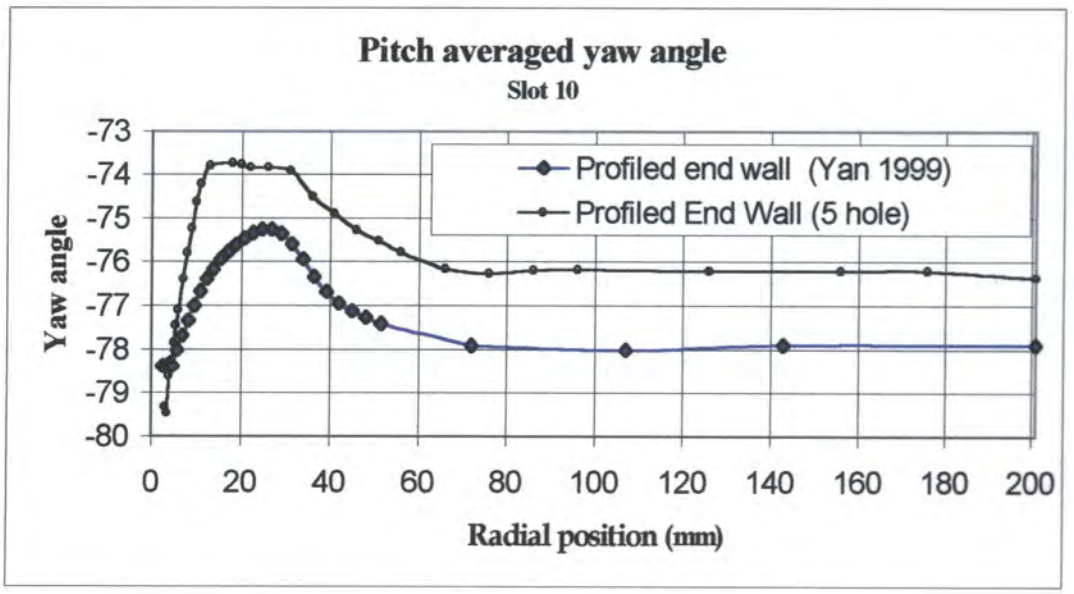

Figure 4.19: Profiled end wall pitch averaged data

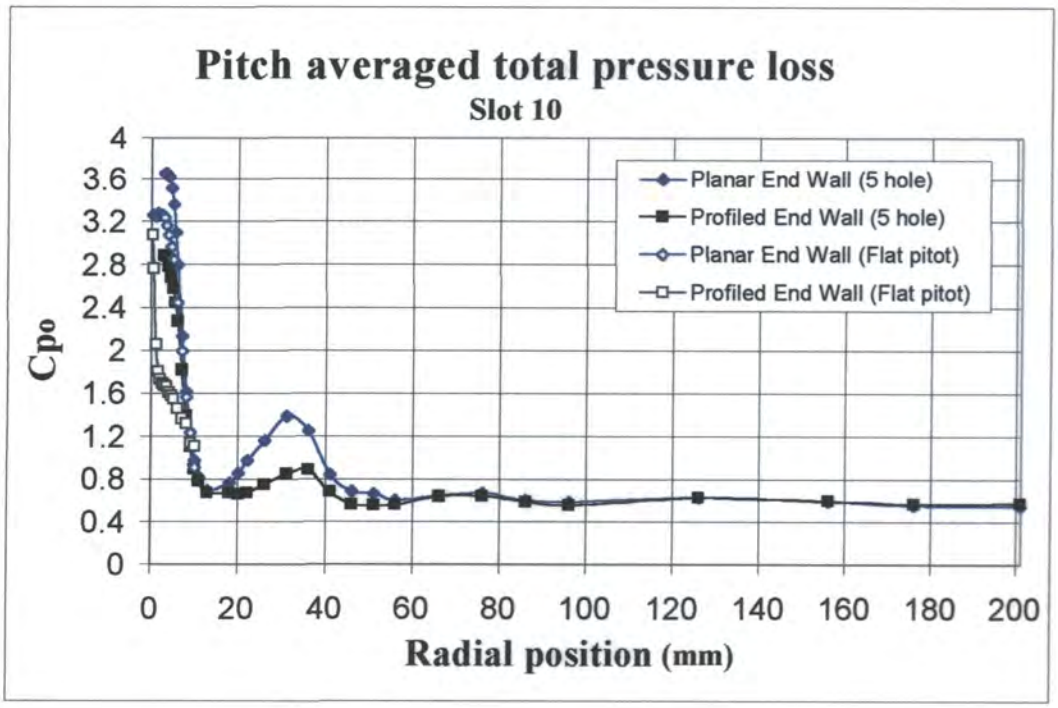

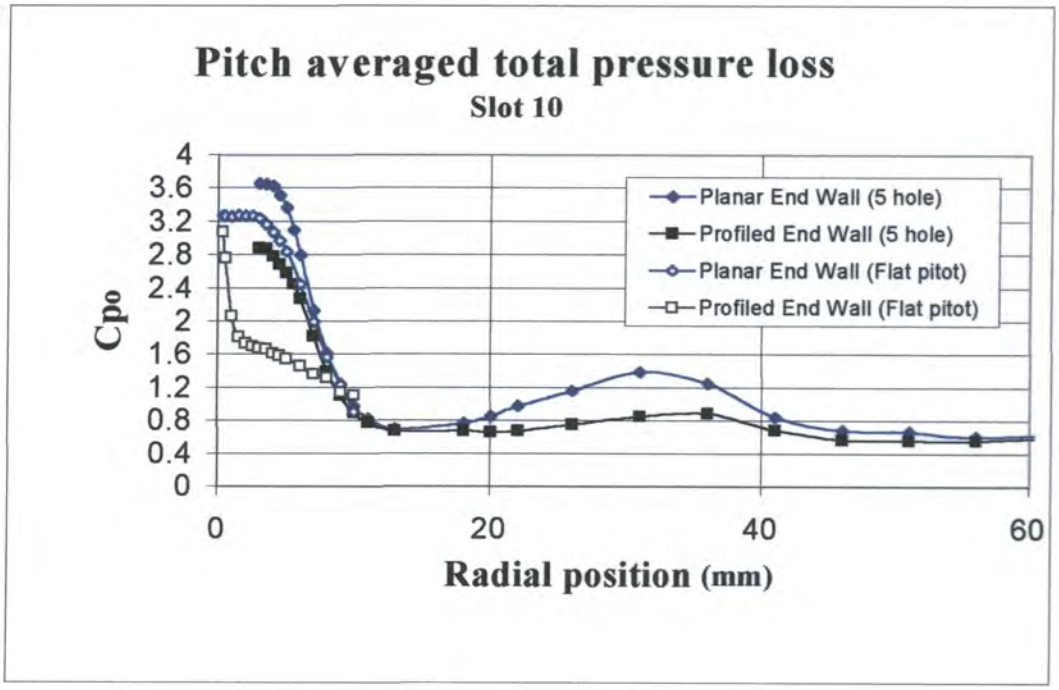

Figure 4.20: Pitch averaged total pressure loss at slot 10

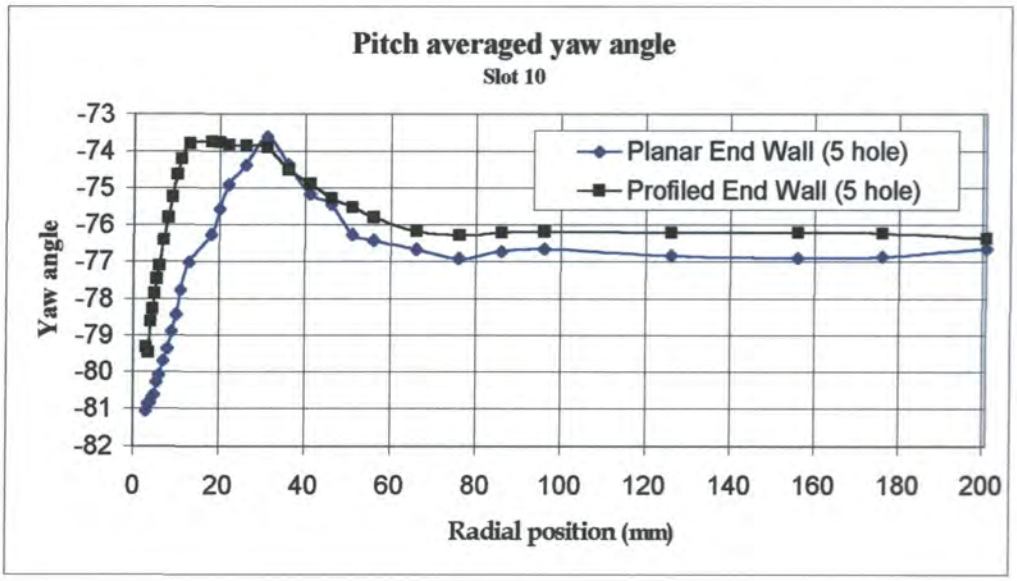

Figure 4.21: Pitch averaged yaw angle

Chapter 5:

Evaluation and Discussion

5.1 Introduction

The aim of this work has been to investigate the effect of the shaped end wall, designed by Yan [1999], on the secondary flow and total pressure loss, in a linear cascade. The main objective was to investigate the effect of the shaped end wall in the area adjacent to the wall, in order to obtain a clear view of the flow and the amount of loss. Previous experimental work by Yan [1999] was carried out with a series of five hole probes whose size did not allow detailed measurements very close to the end wall. The importance of measurements close to the end wall lies in the type of blade used. The high contraction ratio nozzle guide vane was designed in such way that the secondary flow was concentrated in the near end wall region.

Downstream measurements were made close to the end wall using a flattened pitot probe. Moreover as Yan overestimated the loss, half span traverses were made using a finer five hole probe than that previously used, in order to achieve more accurate measurements of the loss. Two slots were traversed downstream using the flattened

pitot probe whereas due to time constrains only slot 10 half span traverses where made, using a five hole probe.

5.2 Experimental results with the flat end wall

In order to investigate the effect of the profiled end wall on the secondary flow the planar end wall was first traversed in order to obtain a reference point. Using the flattened pitot probe slot 09 and slot 10 were traversed covering an area of 10mm adjacent to the end wall. A detailed view of the total pressure loss was achieved. These results are then compared to Yan [1999].

At the first tangential slot downstream (slot 09), the end wall boundary layer is newly formed and its edge is relatively close to the end wall. As seen from slot 09 results (*Figure 4.3*). Yan measured a thickness of approximately 6mm to 7mm, whereas the flattened pitot probe measured a thinner end wall boundary layer, approximately 4.5mm to 5.5mm. The flattened pitot probe at slot 09 has captured the wakes of the two blades and a more detailed view of the loss close to the end wall is achieved, as a much finer grid was used for traversing compared to Yan [1999]. The loss coefficient within the boundary layer shows a higher peak measured by the flattened pitot than that measured by Yan. Due to its small size the flattened pitot probe value is believed to be more accurate. Additionally the loss coefficient at the base of each wake is higher than Yan by 0.5 having a value of 4.0 and the wakes are more clearly defined for the area within 10mm from the end wall (*Figure 4.3*).

The pitch averaged results of slot 09 (*Figure 4.4*) show a much lower loss than that mentioned by Yan; although the two sets of data follow the same trend they have a difference in level of loss as seen from the area plots. This difference led to the mid-span traverse shown in *Figure 4.1*.

Slot 10 which is the second tangential slot downstream of the blade row was traversed over the half span distance with the five hole probe as well as close to the end wall with the flattened pitot probe. As expected the end wall boundary layer thickens further downstream and reaches a width of 10mm approximately. The five hole probe and the flattened pitot results agree with Yan [1999] on the increase of the end wall boundary layer thickness as the flow progresses downstream although Yan shows a slightly thicker boundary layer (*Figure 4.8* to *Figure 4.13*). The loss peak close to the end wall in slot 10 is less than that measured at slot 09. Furthermore the flattened pitot measured the lowest peak compared to both the five hole probe and Yan, which agree on the level of loss.

The half-span area plots obtained from the five-hole probe data show a wider wake than that of slot 09 by Yan (*Figure 4.2*). Comparing slot 10 results from Yan with the five hole probe results the most noticeable difference is the wider area of high loss at mid-span and the higher loss within the wakes measured by Yan (*Figure 4.1 Figure 4.8 Figure 4.10)*. The higher mid span loss measured by Yan justified the need of the five hole probe traverse especially as the agreement of the five hole probe traverse data and the flattened pitot probe data is better for both the end wall traverses, as seen from the pitch averaged results.

The bigger five-hole probe used by Yan could be responsible for the higher loss measured. In comparison to the new five hole probe the one used by Yan would have caused more blockage close to the end wall and thus be less accurate. However this alone would not have any significant effect on the loss away from the end wall. Therefore it is believed that a systematic error could also be the cause of the higher loss measured by Yan.

The difference in yaw angle observed between the data by Yan and the five hole probe could be attributed to the different probes used. However the method used by Yan to determine the angle is theoretically more accurate as a calibration map is applied to the pressures measured from the probe, whereas the new data were determined manually as described in Chapter 3. Therefore the two sets of data are influenced by different factors making difficult to determine which of the two is more accurate. It is believed that the two would be in better agreement had the same probe been used or the same method been used in taking measurements.

Slot 09 and slot 10 flattened pitot pitch averaged results show the same trends in loss. A steep reduction in loss is observed for both sets of data. This fact can be regarded as an indication of the repeatability of the experiments and of the accuracy of the pitot probe as in theory there should be such an agreement.

However the flattened pitot probe pitch averaged results show a lower loss than the five hole probe for the first 5mm close to the end wall. The former is believed to be more accurate as the flattened pitot probe is smaller thus causing less blockage. The

effect of using the flattened pitot probe for measurements can clearly be seen in *Table 4.1* looking at the net secondary loss. Using the mixed data the secondary loss is higher than given by both Yan and the five hole probe. However Yan's secondary loss is lower only due to the fact that he measured a higher mid span loss which is used as the profile loss in the calculations.

Dunham [1970] in his review of the secondary losses and the loss correlations concluded that the Ainley and Mathienson [1951] correlation gave the most satisfactory results. *Table 5.1* presents the net secondary loss derived from some of the reviewed correlations in comparison to the secondary loss measured experimentally.

Correlation	**Net secondary loss**
Soderberg 1949	0.8642
Ainley & Mathienson 1951	0.3936
Scholz 1954	0.8052
Markov 1958	0.1001-0.2905
Yan 5 hole probe (Planar end wall)	0.1306
5 hole probe (Planar end wall)	0.1506
Mixed data (Planar end wall)	0.1733

Table 5.1: Net secondary loss based on inlet dynamic head

As seen from *Table 5.1* the correlations cover a wide range of values for the same cascade. These correlations were developed in the 1950's and their accuracy is questionable for modern cascades. However Markov's correlation shows the best agreement with the experimental values.

5.3 Experimental results with the profiled end wall

The profiled end wall was fitted to the cascade and slots 09 and 10 were traversed. The flattened pitot probe showed much better defined wakes than Yan for slot 09 (*Figure 4.5*). The end wall boundary layer thickness is not clearly defined by Yan's data whereas the flattened pitot probe shows a thickness of less than 1mm. The effect of end wall profiling in the area close to the end wall can be clearly seen in slot 09 as the wakes measured with the flattened pitot in *Figure 4.5* are narrower than in those *Figure 4.3* and the loss between the wakes is greatly reduced. Moreover the profile has the effect of reducing the boundary layer thickness. It can be said that the profiled end wall delays the development of the end wall boundary layer exiting the blade row. This effect can be seen in the pitch averaged plots of slot 09 (*Figure 4.7*), where the difference in level of loss is great between profiled and planar end wall data.

Slot 10 half span traverses mark the effect of the profiled end wall on the loss core which is associated with the passage vortex. The core has been shifted by 2mm to 5mm towards the end wall and at its peak, 30mm from the end wall, a reduction in the total pressure loss coefficient of 28% is achieved. The area greatly effected by the end

wall profiling is the area within 60mm from the end wall which shows an overall reduction in loss and a reduction of overturning and underturning as seen from *Figure 4.8* and *Figure 4.14.*

At mid span for both the planar and profiled end wall five hole probe traverses for slot 10 show the same loss whereas Yan shows a higher loss especially within the wakes. Generally Yan has overestimated the loss and presents a wider area of high loss at mid span, justifying the need of the new five hole probe traverses, as the loss level now is now more realistic.

Estimations of the profile loss and the secondary loss were made. The profile loss was based on Ainley and Mathienson [1951] tables for nozzle row profile loss coefficients. For the nozzles used the estimation of profile loss is presented in *Table 5.2* The table shows how the estimated value compares to the experimental results for both profiled end planar end wall. Bearing in mind that the correlation was developed in the 50's its accuracy and agreement with modern day design data is not expected to be high and is only used here as an indication. Furthermore new designs have been developed over the years with minimum profile losses.

Ainley & Mathienson	Yan Planar end wall	Yan Profiled end wall	5-hole probe planar end wall	5-hole probe profiled end wall
0.0500	0.0422	0.04100	0.0264	0.0275

Table 5.2: Profile loss based on inlet dynamic head

The flattened pitot traverse for slot 10 indicates that the profiled end wall has significantly reduced the end wall boundary layer thickness from 9-10mm to 2.5-2mm. A reduction of the mid pitch loss between the wakes is also measured compared to the planar end wall, which is approximately 50% (*Figure 4.18*). The pitch averaged results exhibit the effect of the profiled end wall (*Figure 4.19*). The peak of loss lying between 20mm and 30mm radially is reduced compared to the planar end wall along with the loss close to the end wall. The reduction of the peak loss in the loss core can be attributed to the reduction of the end wall boundary layer and its loss, as this means that less low energy fluid is available to be swept away from the end wall by the cross passage pressure gradient which would be deposited in the loss core associated with the pre-mentioned passage vortex.

Furthermore there is less variation in the measured yaw angle which suggests a weaker passage vortex is formed when the profiled end wall is used (*Figure 4.21*). The reduction in overturning and underturning suggests that the profiled end wall has successfully reduced the cross passage pressure gradient

The mass averaged data of *Table 4.2* make the effect of the profiled end wall more noticeable as the five hole probe data indicate a 48% reduction in net secondary loss whereas the mixed data show a 52% reduction. The data by Yan measured a reduction of only 23% of the secondary loss.

Based on the experimental results with the use of new smaller and more accurate probes it is believed that a more accurate measurement of loss was achieved by the new data the end wall profiling proves more advantageous than earlier research by Yan indicated.

Although various factors contribute to an error in the Cp_o measurement, as presented in section 3.3., the overall level of error is still much lower than the gain obtained by using the profiled end wall. Not only the profiled end wall presents a significant reduction of the total pressure loss, but the new series of traverses show a greater reduction than that presented by Yan. As it is shown in *Table 4.2* the mixed data values of the net secondary loss show a reduction of nearly 52% compared to 23% presented by Yan. Assuming the total error was to sum up to $\pm 5\%$, this is still small compared to the difference between Yan's data and new traverses, as the magnitude of the loss reduction is far greater

Chapter 6: Conclusions and further work

6.1 Introduction

This chapter aim is to present the main conclusions drawn from the experimental work carried out for both planar and profiled end wall. The flow field downstream of the blade passage was investigated and the results were compared to previous work carried out on the same cascade. Additionally some suggestions for further work that could improve the accuracy of the results are part of this chapter

6.2 Conclusions from experimental work

1) The flow field was investigated with a five hole probe designed by Hartland [1999], which provided reasonable results. The smaller sized probe allowed measurements closer to the end wall than Yan had achieved with the five hole

probe he used. The new five hole probe used caused less blockage close to the end wall than the probe originally used by Yan which would make it more accurate closer to the end wall. Nevertheless the accuracy of the probe closer than 8mm to the end wall is questionable (*Figure 4.20*).

2) The flattened pitot probe provided a good measurement tool for close to the end wall traverses. The accuracy of the probe is high for small angle deviations. As the probe was set at the mid span flow angle the angle only varied from +6 to –6 degrees which is within the bandwidth of accuracy of the flattened pitot probe. However for mass averaging over the pitch, the angle and static pressure had to be interpolated for the area that was also covered with the flattened pitot probe or extrapolated for locations close to the end wall, which could reduce the accuracy of the results.

3) The experimental results obtained from the cascade and especially the area plots suggested that a good periodicity had been achieved, as the wakes from both the blades in the passage covered are very similar. The position of the wakes appears to be shifted to the left by 10mm compared to Yan but both sets of data show that the wakes are approximately 140mm apart which agrees with the 140mm pitch.

4) Slot 09 was traversed with only the flattened pitot probe. The results obtained differ from Yan in the level of loss as the flattened pitot probe results are showing lower loss. Furthermore the effect of end wall profiling seems greater when measured with the flattened pitot probe than with the five hole probe used by Yan. A bigger difference in loss was measured between planar and profiled

end wall data, than that measured by Yan, whereas the boundary layer thickness is significantly reduced by the profiled end wall.

5) Slot 10 half span data give a good view of the flow field at exit from the blade row. As also indicated in the mid span traverses the total pressure loss was lower than originally measured by Yan. The most noticeable difference lay in the loss peak 30mm to 40mm in the radial direction as well as in the overall level of loss. The yaw angle data for both Yan and the five hole probe were in good agreement regarding the trend followed, although there was an angle level difference possibly arising from the different probes and measuring techniques used. However the new five hole probe data showed increased overturning and underturning for the planar end wall compared to Yan.

6) The profiled end wall as measured with the five hole probe has no significant effect on the flow at mid span. The area that suggests a significant reduction in loss compared to the planar end wall data lies within 60mm from the end wall. The overturning and underturning has been reduced by the profiled end wall, especially in the areas associated with the passage vortex and a lower loss peak is measured at 40mm radially. Closer to the end wall the overturning has also been reduced and the growth of the boundary layer thickness has been restricted, thus lowering the loss close to the end wall.

7) Comparing the flattened pitot data to the five hole probe data for slot 10 there is agreement at 10mm from the end wall. The flattened pitot probe gives lower loss for the first 4.5mm for the planar end wall than the five hole probe whereas the

slope of the pitch averaged results is reduced. Thus a higher area averaged loss is measured with the flattened pitot probe than with the five-hole probe. The profiled end wall flattened pitot data are constantly lower than the corresponding five hole probe data allowing a more significant reduction of the secondary loss to be made by the profiled end wall. The mixed data values show that the profiled end wall is more advantageous than predicted by the five-hole probe. The loss is less compared to Yan but also a further reduction is present close to the end wall that both the five hole probes would not detect due to their size and the increased blockage caused compared to the flattened pitot. Using the flattened pitot probe the secondary loss appears to be further reduced by 3% compared to the new five hole probe data which shows that the reduction in secondary loss is almost twice that measured by Yan.

8) The level of error, which at its maximum could add up to 5%, has little significance compared to the overall effect of the profiled end wall as presented in this thesis. The gain achieved by using end wall profiling is several times higher than the maximum error, which still has little significance even if compared to the difference in gain between results presented by Yan and the author.

6.3 Future work

After the completion of the work described in this thesis some suggestions can be made for work that could be developed in the future.

1) The flow field within the blade passage could be investigated with a new five hole probe as it is believed that the loss was overestimated by Yan and the profiled end wall could prove more advantageous.

2) The pressure transducers used should be rechecked and if needed re-calibrated or replaced as their accuracy for the yaw angle measurements was questionable. Furthermore an attempt should be made to redesign the data acquisition system so that the length of the tubing connecting the probe and the transducers is reduced, which allow more accurate and less time consuming measurements to be made.

3) The scale of the cascade could be made bigger as the investigation of the flow close to the end wall, where the profile has its more significant effect, would be made easier, as the five hole probes would cause less blockage.

4) The probe calibration rig could be improved by using different and more accurate transducers. Furthermore a different configuration of the air pump could improve the probe calibration as the current configuration introduces some unsteadiness in the flow.

5) The shaped end wall was only tested in a linear cascade. The effect of the profile should also be investigated in an annular cascade or in a model turbine where the flow is more complicated. Furthermore multiple blade rows could be tested in order to understand the full effect of end wall profiling on the overall

performance of a turbine. The more uniform exit flow angle could give extra benefits in a succeeding rotor row

References

Ainley, D.G., and Mathienson, G.C.R., 1952. "A Method of Performance Estimation for Axial Flow Turbines", NGTE Report R111.

Atkins, M.J., 1987. "Secondary Losses and End-Wall Profiling in a Turbine Cascade", IMechE. Conf. Proc. C255/87, pp.29-41

Came, P.M., 1973, "Secondary Loss Measurements in a Cascade of Turbine Blades", IMechE Proceedings London, Conference Publication 3,

Came, P.M., and March, H., 1974, "Secondary Flows in Cascades; two simple Derivations for the Components of Vorticity", Journal of Mechanical Engineering Science.

Chen, L.D., and Dixon S.L., 1986, "Growth of Secondary Flow Losses Downstream of a Turbine Blade Cascade", Journal of Engineering for Gas Turbine and Power, Vol. 108. Pp. 270-276

Deich, M.E., 1960, " Method of Increasing the Efficiency in Turbine Stages", Teploenergetica No. 2, February 1960, Translation No. 2816.

Dejc, M.E., 1973, "Untersunchung Und Berechnung Axialer Turbinstufen", Berlin, VEB Verlag Technik,

Denton, J.D., 1993, "Loss Mechanisms in Turbomachines", ASME, Paper No 93-GT-435.

Dominy, R.G., and Harding, S.C., 1990, "An Investigation of Secondary Flows in Nozzle Guide Vanes", Proc. 74th Specialists' Meeting, Propulsion and Energetics Panel, NATO AGARD-CP-469, pp.7.1-7.15

Duden, A. et. al., 1998, " Controlling the Secondary Flow in a Turbine Cascade by 3D Airfoil Design and Endwall Contouring", ASME, Paper No. 98-GT-72.

Dunham, J., 1970, "A Review of Cascade Data on Secondary Losses in Turbines", IMechE, J. Mech. Eng. Sci. Vol. 12, No. 1, pp.48-59

Dunham, J., and Came, P., 1970, "Improvements to the Ainley-Mathienson Method of Turbine Performance Prediction", ASME transactions, Series A, 92,

Govardhan, M., 1986, "Secondary Losses in a Large Deflection Annular Turbine Cascade: Effect of the Entry Boundary Layer Thickness", ASME, Paper No. 86-GT-171.

Gregory-Smith, D.G., and Besigner, T.E.,1993, "Reduction in Secondary Flows and Losses in a Turbine Cascade by Upstream Boundary Blowing", ASME, Paper No.93-GT-114.

Gregory-Smith, D.G., 1982, "Secondary Flows and Losses in Axial Flow Turbines", ASME, Paper No. 82-GT-19.

Gregory-Smith, D.G., and Walsh J.A., 1987, " The Effect of Inlet Skew on the Secondary Flows and Losses in a Turbine Cascade", IMechE, C275/87.

Gregory-Smith, D.G., and Graves C.P., 1983, " Secondary Flow Losses in a Turbine Cascade", AGARD-CP-351 pp. 17.1-17.24.

Gregory-Smith, D.G., 1997 "Secondary and Tip Clearance Flows in Axial Turbines", Von Karman Institute for Fluid Mechanics, Lecture Series 197-01

Gustafson, B.A., 1977, "Some Observations from Low-Speed Cascade Tests Concerning Side Wall Boundary Layer Suction", AGARD-CP-214.

Haller, B.R., 1997, "Secondary and Tip-Clearance Flows in Axial Turbines: Full 3D Blade Design", Von Karman Institute Lecture series 197-01,

Harrison, S., 1989, "Secondary Loss Generation in a Linear Cascade of High-Turning Turbine Blades", ASME, Paper No. 89-GT-47.

Harrison, S., 1990, "The Influence of Blade Lean on Turbine Losses", ASME, Paper No. 90-GT-55

Hartland, J.H., 1998, "Non-Axisymetric Endwall Profiling in a Turbine Rotor Blade", ASME 98-GT- 525

Hartland, J.H., Harvey N.W., Rose, M.G., Taylor, M.D.,1999, "Non-Axisymetric Turbine End Wall Design: Part 1 Three-Dimensional Linear Design System", ASME, 99-GT-338

Hawthorne, W.R., 1955, "The Growth of Secondary Circulation in Frictionless Flow", Proc. Camb. Phil. Soc., Vol. 206, pp.374-387

Hodson, H.P., and Dominy, R.G., 1986, " The Off-Design Performance of a Low Pressure Turbine Cascade", ASME, June 8-12, 1986, Paper No. 86-GT-188.

Kawai, T., 1989, "Secondary Flow Control and Loss Reduction in a Turbine Cascade Using Endwall Fences", JSME International Journal, Series II. Vol. 32 No. 3, pp375-387

Kopper, F.C, and Milano, R., 1980, "An Experimental Investigation of Endwall Profiling in a Turbine Vane Cascade", Paper No. AIAA-80-1089.

Marchal, P., and Sieverding, C.H., 1977, "Secondary Flow Within Turbomachinery Bladings", AGARD-CP-214 Paper No. 11

Morris, A.W.H., and Hoare, R.G., 1975, "Secondary Loss Mechanism in a Cascade of Turbine Blades With Meridional Wall profiling", ASME, Paper No. 75-WA-/GT-11

Prumper, H, 1975, "Boundary Layer Effects on Turbomachines", AGARD-AG-164.

Rose, M.G., 1994, "Non-Axisymetric Endwall Profiling in the HP NGV's of an Axial Flow Gas Turbine", ASME Paper No. 94-GT-249.

Sieverding, C.H., 1975, "Reduction of Secondary Losses in Turbines", Von Karman Institute of Fluid Dynamics, Lecture Series 72.

Sieverding, C.H., and Van Den Bosche, P., 1983, "The use of Coloured Smoke to Visualize Secondary Flows in a Turbine Blade Cascade", J. Fluid Mechanics 134, pp. 85-89.

Sieverding, C.H., 1985, "Recent Progress in the Understanding of Basic Aspects of Secondary Flows in Turbine Blade Passages", Journal of Engineering for Gas Turbine and Power, Vol. 107

Squire, H.B., and Winter, K.G., 1951, "The Secondary Flow in a Cascade of Airfoils in a Non-Uniform Stream", Journal of Aerodynamic Science Vol. 18, pp. 271-289

Yamamoto, A., and Nouse, H., 1988, "Effects of Incidence on Three-Dimensional Flows in a Linear Turbine Cascade", ASME, Paper No. 88-GT-110

Yan, J., Gregory-Smith, D.G., Ince, N.Z., 1999a, "Profiled End-wall Design for a Turbine Nozzle Row", IMechE, 1999, C557/060

Yan, J., Gregory-Smith, D.G., Walker, P.J., 1999b, " Secondary Flow Reduction in a Nozzle Guide Vane Cascade by Non-Axisymetric End-wall Profiling", ASME, 99-GT-339

Yan, J., 1999, "The Effect of End Wall Profiling on Secondary Flow in Nozzle Guide Vanes", Ph.D. Thesis, University of Durham.

Waterman, W.F., Tall, W.A. 1976, " Measurements and Prediction of 3-D Viscous Flows in Low-Aspect-Ratio Turbine Nozzles", ASME, Paper No. 76-GT-73

Appendix

1.Area Traverse Coefficients

Total pressure loss coefficient

$$C_{po} = \frac{Po_u - Po_1}{\frac{1}{2}\rho v_u^{\,2}}$$

Static pressure loss coefficient

$$C_p = \frac{P_u - P_1}{\frac{1}{2}\rho v_u^{\,2}}$$

2.Pitch Averaged Coefficients

Total pressure loss coefficient

$$\overline{C}_{po} = \frac{\int v_x C_{po1} dy}{\int v_x dy}$$

Yaw angle

$$\overline{\alpha} = \arctan\frac{\int v_x v_y dy \cdot s}{\left(\int v_x dy\right)^2} = \arctan\frac{\overline{v}_y}{v_x}$$

3. Area Averaged Coefficients

Total pressure loss coefficient

$$C_{po} = \frac{\iint v_x C_{pd} dydz}{\iint v_x dydz} = \overline{\overline{C}}_{pd}$$

Exit Angle

$$\alpha = \arctan \frac{\iint v_x v_y \, dydz \cdot \rho^2 \cdot h \cdot s}{\left(\iint v_x \, dydz \right)^2} = \arctan \frac{\overline{\overline{v_y}}}{\overline{\overline{v_x}}} = \overline{\overline{\alpha}}$$